Universidad de Concepción
Dirección de Postgrado
Facultad de Ciencias Biológicas
Programa de Doctorado en Ciencias Biológicas
Área Biología Celular y Molecular

**TESIS PARA OPTAR AL GRADO DE DOCTOR EN CIENCIAS BIOLÓGICAS
ÁREA BIOLOGÍA CELULAR Y MOLECULAR**

FUNCTIONAL AND STRUCTURAL ANALYSIS OF *ANDES VIRUS* L PROTEIN N-TERMINAL DOMAIN, A POTENTIAL PHARMACOLOGICAL TARGET.

"ANÁLISIS FUNCIONAL Y ESTRUCTURAL DEL DOMINIO N-TERMINAL DE LA PROTEÍNA L DE *ANDES VIRUS*, UNA POTENCIAL DIANA FARMACOLÓGICA."

YAIZA FERNÁNDEZ GARCÍA
CONCEPCIÓN-CHILE
2016

Profesor Guía: Dr. Oliberto Sánchez Ramos
Dpto. de Farmacología, Facultad de Ciencias Biológicas
Universidad de Concepción-Chile

Profesor Co-Guía: Dra. Sophia Reindl
Dpto. de Virología
Bernhard Nocht Institute for Tropical Medicine-Alemania

Esta tesis ha sido realizada en el Departamento de Farmacología de la Facultad de Ciencias Biológicas, Universidad de Concepción-Chile y el Departamento de Virología del Bernhard Nocht Institute for Tropical Medicine-Alemania.

Profesores integrantes Comisión Evaluadora:

_____
Dr. Oliberto Sánchez Ramos
Profesor Guía
Facultad de Ciencias Biológicas

_____
Dra. Sophia Reindl
Profesor Co-Guía
Bernhard Nocht Institute for Tropical Medicine

_____
Dra. Marta Bunster Balocchi
Facultad de Ciencias Biológicas

_____
Dr. Sergio Oñate Betancour
Facultad de Ciencias Biológicas

_____
Dr. Marcelo Cortez San-Martín
Profesor Evaluador Externo
Universidad de Santiago de Chile

_____
Dr. Juan Pablo Henríquez H.
Director
Programa Doctorado en Ciencias Biológicas
Mención Biología Celular y Molecular

To Erick, my better half…

ACKNOWLEDGEMENTS

- To Dr. Sophia Reindl, for introducing me to the field of structural biology, taking me in her research group and close supervision of this work.

- To Dr. Stephan Günther, for receiving me in the Department of Virology at the Bernhard-Nocht-Institute for Tropical Medicine (BNITM) – Germany.

- To Dr. Oliberto Sánchez, for receiving me in the Department of Pharmacology at the University of Concepcion (UdeC) – Chile.

- To CONICYT, for funding through PhD. Fellowship 21110444 and PhD. Internship 2014-7571.

- To MECESUP, for funding through Project UCO 1311.

- To FONDECYT, for funding through Project 1110925.

- To the Graduate School from the University of Concepcion, for financial aid.

- To Dr. Marta Bunster, Dr. Sergio Oñate and Dr. Marcelo Cortez, for the critical reading of this document.

GENERAL CONTENT

FIGURES CONTENT

TABLES CONTENT

I. ABSTRACT

Andes virus (ANDV) is the main etiological agent of hantavirus cardiopulmonary syndrome in South America. Like other segmented negative-ssRNA viruses, ANDV initiates its mRNA synthesis by using cap structures derived from host cell mRNAs. The nuclease motif PD…(E/D)…K present in the N terminus of the L protein, one of four proteins encoded by the viral genome, is believed to act in the cap-snatching mechanism. However, in addition to the complete lack of sequence similarity to previously described endonucleases there is no experimental evidence of a functional enzyme for this region within the large protein.

In order to study the function and structure of ANDV L protein N-terminal domain and due to toxicity of the wild-type protein in bacteria, mutants were produced and biochemically assessed. It was shown that the first 200 amino acids exhibit a Mn^{2+} ion dependent endoribonuclease activity. Such activity neither required of cap structures nor specific sequences. Furthermore, the first tridimensional arrangement of atoms of a hantaviral endonuclease domain was solved at a resolution of 2.4Å. The structure revealed an evolutionary conserved protein fold with distinct positively charged patches surrounding the active site. As proof of concept and to expose the utility of mutants with catalytic activity in future antiviral screenings, a dose-dependent reduction of the *in vitro* enzymatic activity was demonstrated using a typical inhibitor of cap-snatching endonucleases. Thus, the following study characterized functionally and structurally an attractive pharmacological target and proposes tools that will allow for the development of therapeutic strategies against hantaviruses infections.

II. RESUMEN

Andes virus (ANDV) es el principal agente etiológico del síndrome cardiopulmonar causado por hantavirus en Sudamérica. Al igual que otros virus con genomas segmentados de ARN monocatenario, ANDV inicia la síntesis de su ARNm usando caperuzas derivadas de los ARNm de la célula huésped. El motivo nucleasa PD…(E/D)…K presente en el extremo amino terminal de la proteína L, una de las cuatro proteínas codificadas por el genoma viral, se cree que actúa en el mecanismo de "cap-snatching". Sin embargo, además de la completa ausencia de similitud de secuencia con otras endonucleasas identificadas anteriormente no existe evidencia experimental de una enzima funcional en esta región de la larga proteína.

Con el objetivo de estudiar la función y estructura del dominio N-terminal de la proteína L de ANDV y dada la toxicidad de la proteína de tipo silvestre en bacterias, se produjeron mutantes y éstas se evaluaron bioquímicamente. Se mostró que los primeros 200 aminoácidos exhiben una actividad endoribonucleasa dependiente de Mn^{2+}. Dicha actividad no requirió de caperuzas ni de secuencias específicas. Adicionalmente, este trabajo resolvió a una resolución de 2.4Å la primera disposición tridimensional de átomos para un dominio endonucleasa de hantavirus. La estructura reveló una conformación proteica conservada evolutivamente con distintivos parches cargados positivamente rodeando el sitio activo. Como prueba de concepto, para exponer la utilidad de las mutantes con actividad catalítica en futuras pesquisas de antivirales, empleando un inhibidor típico de "cap-snatching" endonucleasas se demostró una reducción dosis-dependiente de la actividad enzimática *in vitro*. De esta forma el siguiente estudio caracterizó funcional y estructuralmente una atractiva diana farmacológica y propone herramientas que permitirán el desarrollo de estrategias terapéuticas contra infecciones por hantavirus.

III. INTRODUCTION

III. 1. *Andes virus* as an etiological agent

Andes virus (ANDV) is the main source of hantavirus cardiopulmonary syndrome (HCPS) in South America. The geographic distribution and epidemiologic patterns of associated outbreaks reflects the occurrence of its natural reservoirs. Therefore, favorable environmental conditions for the hosts populations, as food abundance during rainy season, are linked to the sporadic and clustered appearances of HCPS cases (Jonsson et al. 2010; Nsoesie et al. 2014).

Although, historically associated to rodent *Oligoryzomys longicaudatus*, its asymptomatic detection in multiple species has recently led to question the diversity of nidus, co-speciation and host switching events during evolution (Ramsden et al. 2009; Rivera et al. 2015). ANDV is horizontally transmitted among rodents through exposure to excreta and saliva of infected animals. Infection of reservoirs results in high viremia within 2 weeks, followed by dissemination of the virus throughout the animal and a persistent infection with prolonged shedding. Persistence has been found related to an increased regulatory T cells that modulate the immune response and prevent clearance of infected cells (Easterbrook & Klein 2008).

Apart from the usual transmission route from reservoirs to humans, by inhalation of dust particles contaminated with infectious excreta, person-to-person transmission has been reported for ANDV (Martinez-Valdebenito et al. 2014). Thus, controlling secondary transmission becomes problematic and patient isolation together with barrier nursing is highly recommended.

Human ANDV infections frequently result in HCPS. Incubation periods are believed to range from 2 to 5 weeks, during which viral RNA can be detected in peripheral blood, accompanied by a prodrome phase and rapid onset of acute disease (Vial et al. 2006). The prodrome phase typically lasts 4 to 7 days and often includes unspecific symptoms as fever, myalgia, malaise, headache and gastrointestinal disorders. Acute clinical features promptly appear as a severe respiratory disease with bilateral pulmonary infiltrates, pleural effusions and hypotension, which can lead within 3 to 5 days to cardiogenic shock and death in almost 40% of the cases. Recovery of surviving patients is remarkably quick, with rapid clearance of the virus and resolution of lesions in a week. A close resemblance to the progression and pathology of HCPS is observed in Syrian hamsters after infection with ANDV, which makes it an excellent animal model (Hooper et al. 2001; Campen et al. 2006).

Regardless of the disease outcome exhibited in different rodents and humans, ANDV targets endothelial cells with the highest concentrations of virus in the lungs. In the absence of virus-induced cytolysis, a strong suppression of regulatory T-cells in ill subjects contributes to a localized immune response that accounts for an increased vascular permeability with capillary leakage (Safronetz et al. 2011; Vaheri et al. 2013). Interestingly, the induction of virus-specific antibodies correlates with the cessation of viremia in hosts with stark contrast to the onset of symptoms in the animal model and humans (Fig.1.) (Spengler et al. 2013; Hooper et al. 2001; Vial et al. 2006).

Due to the involvement of immune mechanisms in HCPS, retrospective studies have suggested the use of genetic markers like specific interleukin 28B (IL28B) haplotypes as predictors of the clinical evolution in ANDV infected patients (Angulo et al. 2015). This tool becomes useful for individuals at permanent risk of exposure as are scientists or medical staff in contact with the virus and workers in rural areas with previous outbreaks.

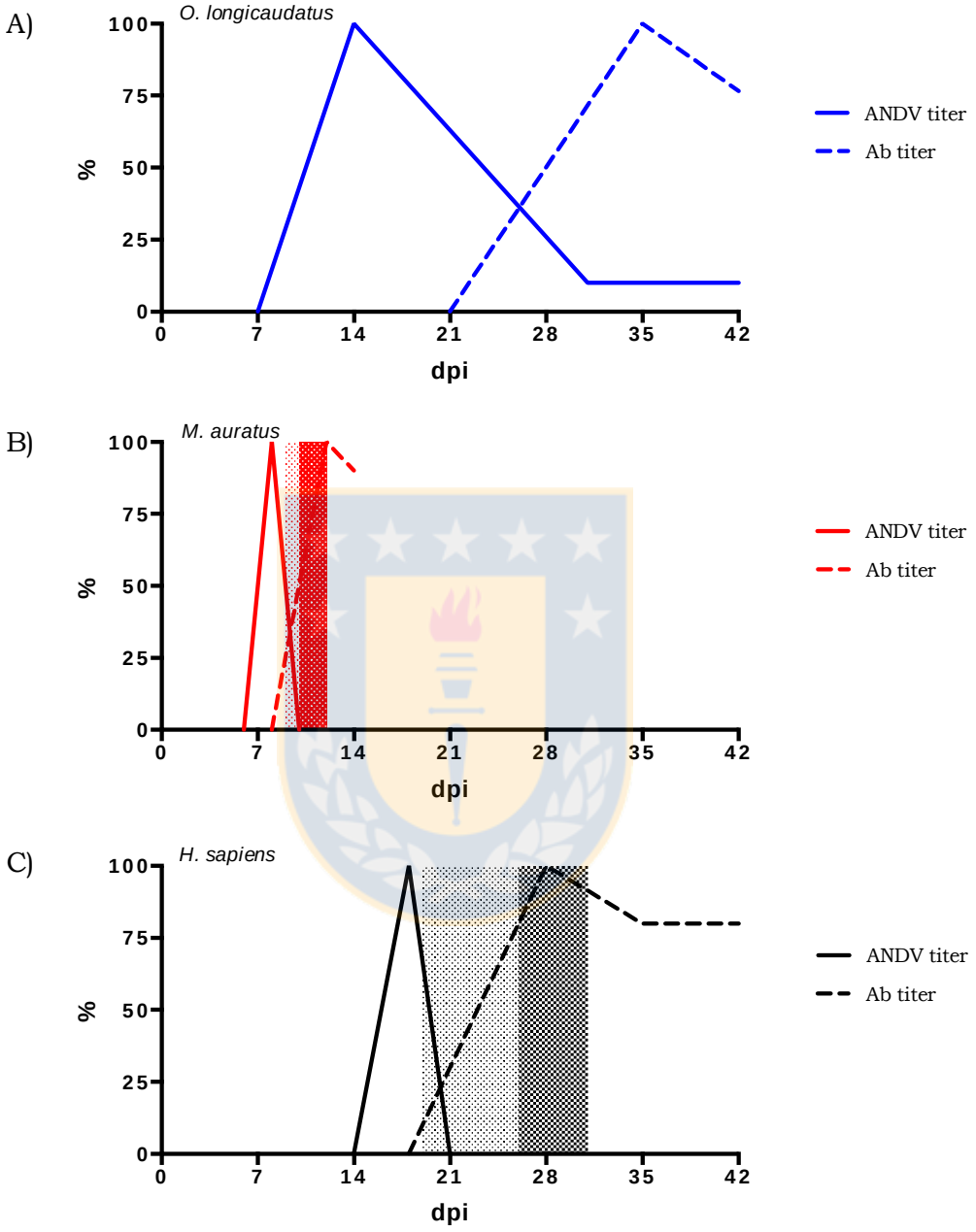

Fig.1. Dynamics of ANDV infection in A) reservoir *O. longicaudatus* (Padula et al. 2004), B) animal model *M. auratus* (Hooper et al. 2001) and C) HCPS patient *H. sapiens* (Vial et al. 2006). Characteristic serum titers of ANDV and virus-specific antibodies (Ab) are shown as percentages relative to their maximum value. Prodrome and acute phases of the disease are indicated as light and dark patterns respectively. dpi: days post-infection.

Differential diagnosis of HCPS can be difficult at early stages due to unspecific symptoms. Hospital admission of mild and severe cases often occurs with the appearance of dyspnea and hypoxemia during the acute phase of the disease. Confirmation of the initial diagnosis is commonly based on serologic tests which detect IgM/IgG antibodies against cross-reactive structural proteins of hantaviruses by enzyme-linked immunosorbent assay (ELISA), indirect fluorescent antibody test (IFA) or immunoblot methods (Mattar et al. 2015). To identify the causative virus, detail genetic information is needed and reverse transcription-polymerase chain reaction (RT-PCR) techniques have been used for this purpose. While successful ANDV isolation has been accomplished from reservoirs and asymptomatic humans, attempts from acute clinical specimens frequently fail (Meissner et al. 2002; Galeno et al. 2002). It is believed that the immune response present at the time of the sample collection hinders the rescue of the virus. Therefore, viral culture is not considered for diagnostics.

To date, there are no approved prophylactic or therapeutic strategies against HCPS. Pre-clinical testing of DNA vaccine candidates encoding ANDV envelope glycoproteins have shown to be safe and elicit high-titers of protective neutralizing antibodies in diverse animal models (Custer et al. 2003; Hooper et al. 2006; Kwilas et al. 2014). However, licensure of any DNA vaccine for human use in the coming years remains elusive. Treatment options based on immunomodulators or non-specific antivirals, like methylprednisolone and ribavirin (RBV) respectively, have been employed in clinical trials without success (Vial et al. 2013; Moreli et al. 2014). Albeit promising animal experiments have revealed post-exposure protection by neutralizing antibodies produced in geese or bovines, a controlled human clinical trial using intravenous infusion of convalescent immune plasma conferred a borderline significance in the case fatality ratio (Haese et al. 2015; Hooper et al. 2014; Vial et al. 2014). Moreover, the aforementioned approach holds large probabilities of resistance to treatment due to the intrinsic relative high mutation rates of external proteins (Ramsden et al. 2008). As general rule, the experience

gathered with the development of drug resistance by all *Influenza virus* (IFV; family *Orthomyxoviridae*) genera has led to target proteins less prone to change as the ones forming the viral minimal machinery for transcription and replication (Monod et al. 2015).

III. 2. Molecular biology of hantaviruses

ANDV belongs to the genus *Hantavirus*, 1 of 5 genera composing the *Bunyaviridae* family. Together with their shared antigenic properties, hantaviruses are enveloped virions of 80-120 nm of diameter containing a tri-segmented single-stranded RNA (ssRNA) genome with negative polarity which replicates in the cytoplasm.

The viral genome segments are designated according to size as S (~1.9 kb), M (~3.7 kb) and L (~6.6 kb). Each one accommodates an open reading frame (ORF) flanked by noncoding regions (NCR) harboring regulatory elements. The 3´ and 5´-monophosphorilated termini, which act as the viral promoters, include tri-nucleotide repeats in highly conserved sequences within the genus that are complementary to each other (Garcin et al. 1995). Even though the predicted base-pairing in this region was initially thought to generate a stable panhandle structure responsible for the circularization of the segments (Mir et al. 2006), a more likely *in vivo* scenario has been propose based on protein-RNA interactions (Gerlach et al. 2015). A handful of proteins are synthesized from the viral RNA (vRNA). The S segment encodes for the multifunctional nucleoprotein (NP) and in some viruses, as the result of alternative start codon recognition by ribosomes, for a non-structural protein (NSs) with reported interferon antagonist activity (Kaukinen et al. 2005; Vera-Otarola et al. 2012; Jääskeläinen et al. 2007). The M segment encodes for the glycoproteins precursor co-translationally cleaved into G_N and G_C, which are embedded in the surface of the virions as spikes made up of tetramers of G_N/G_C heterodimers (Hepojoki et al. 2010). Meanwhile, the L segment encodes for the 250kDa L

protein in charge of the viral RNA-dependent RNA-polymerase (RdRp) reactions (Kukkonen et al. 2004). Every segment is packaged along with multiple units of NP and a single L molecule to form ribonucleoprotein (RNP) complexes that, when observed using electron microscopy, give the appearance of coiled beads (Reguera et al. 2014). Given that these complexes comprise the elements sufficient for viral RNA synthesis, they are considered the basic functional entities for transcription and replication. The compacted genome is wrapped by a 5nm thick bilipid membrane covered with spikes protruding approximately 10nm from the surface to create the viral particles (Fig.2.A) (Huiskonen et al. 2010).

The life cycle of hantaviruses takes place in the cytoplasm of infected cells (Fig.2.B). The spike projections displayed in the facade of the viral particles bind to host-cell receptors, like β1 or β3 integrins, triggering a clathrin-mediated endocytosis (Gavrilovskaya et al. 2002; Jin et al. 2002). Once the endocytic vesicles lose their clathrin coat they fuse to early endosomes. The progressive acidification of these organelles promotes conformational changes within the G_N/G_C complexes that enable the merger of the viral and endosome membranes (Ogino et al. 2004). It is believed that the viral genome, in the context of RNPs, released into the cells cytoplasm is transported by components of the cytoskeleton to areas known as viral factories (Ramanathan & Jonsson 2008; Vaheri et al. 2013). Through the association of membranes from the nucleus, endoplasmic reticulum (ER) and cis-Golgi, such factories provide all items required for the transcription of viral mRNAs, their translation, replication of the viral genome and assembly of virions (Fontana et al. 2008). At least a copy of each segment is needed for the production of infectious particles. Their recruitment to the assembly site is achieved by contact with the cytoplasmic tails of either or both of the viral glycoproteins (Battisti et al. 2011). Nevertheless, is not clear how the viral genome is organized to accomplish the appropriate mix of segments. Despite reports of virus maturation at membranes

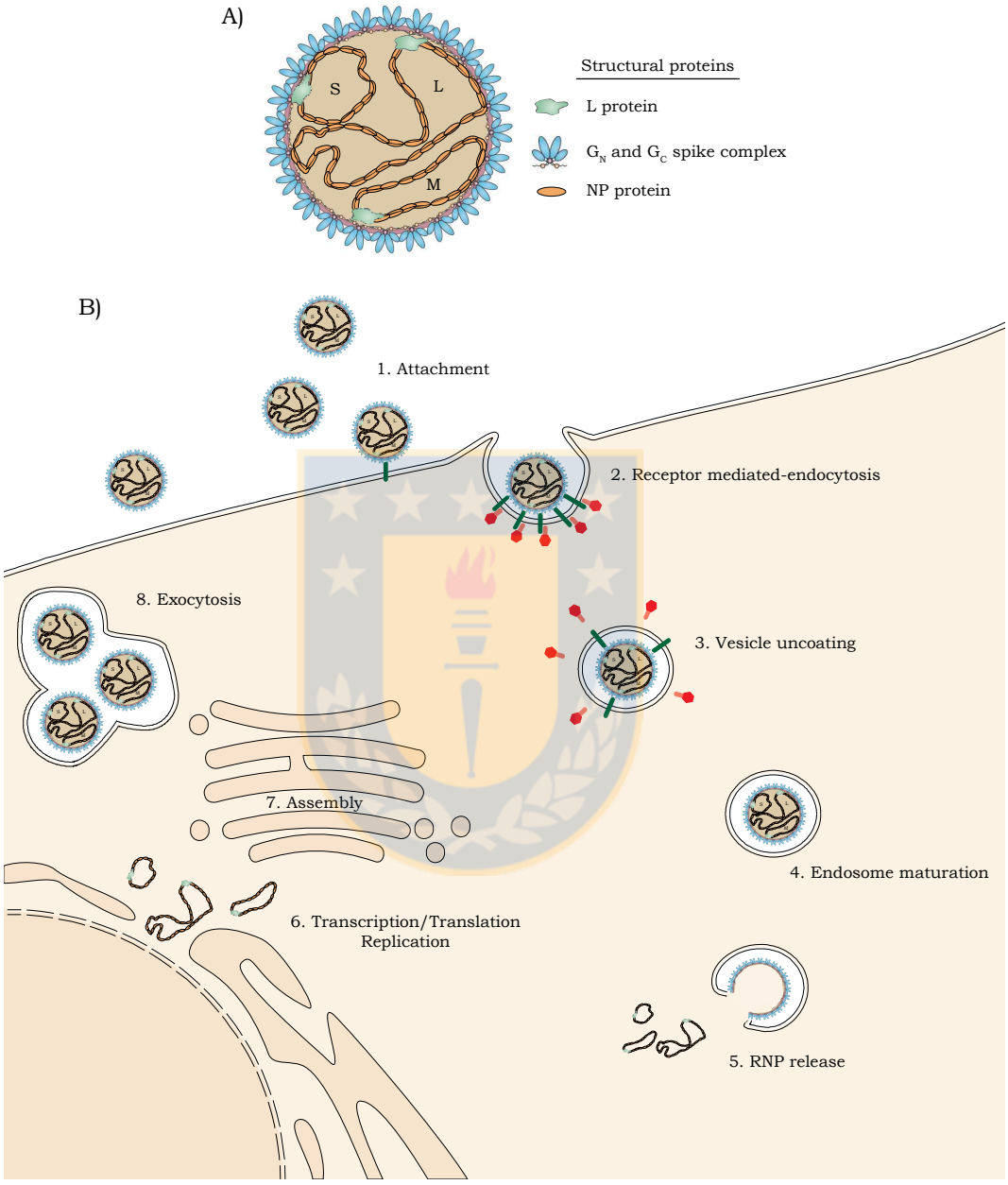

Fig.2. Schematic representation of hantaviruses A) viral particle and B) life cycle. Modified from (Vaheri et al. 2013).

other than those related to the Golgi apparatus (Ravkov et al. 1997), the examination of oligosaccharides attached to G_N and G_C strongly suggest budding of the new viral particles from the cis-Golgi compartment (Shi & Elliott 2004). Finally, virions are mobilized to recycling endosomes for subsequent exocytosis (Rowe et al. 2008).

Hantaviruses utilize RNPs as the foundation for the synthesis of all their RNA species (Reguera et al. 2016). This implies a pre-initiation state where NPs must transiently detach to give the virion-associated L protein access to the template. The initiation step of RNA synthesis during transcription or replication follows a prime-and-realign mechanism (Fig.3). However, the substrates used to commence the reaction vary between both processes. Briefly, the starting material pairs off internally to the 3´-end AUC-tandem sequences within the RNA template. After extension of a few nucleotides, the emerging chain realigns by slippage backwards of the L protein in virtue of the terminal sequence repeats and then continues with the elongation step (Garcin et al. 1995).

Evidence of a stretch of heterologous nucleotides at the 5´-end of hantaviruses mRNAs insinuates the use of capped oligonucleotides cleaved from the host-cell mRNAs as the starting point for transcription (Cheng & Mir 2012). Such phenomenon, known as “cap-snatching”, was originally described for IFV (Bouloy et al. 1978). Here, the PB2 viral protein binds to the 5´-cap of cellular mRNAs and these are cleaved several nucleotides downstream by the PA viral endonuclease. Then the resulting RNA fragments are used as primers to initiate transcription of the viral mRNA by the PB1 protein (Reich et al. 2014). Structural insights from the L protein of related bunyaviruses denotes its ability to adopt multiple conformational arrangements necessary for assorted tasks during the cap-primed RNA synthesis (Gerlach et al. 2015; Das & Arnold 2015).

In order to produce fully transcribed viral mRNAs, it is alleged that the transcription and translation processes are coupled (Barr 2007). After the 5´

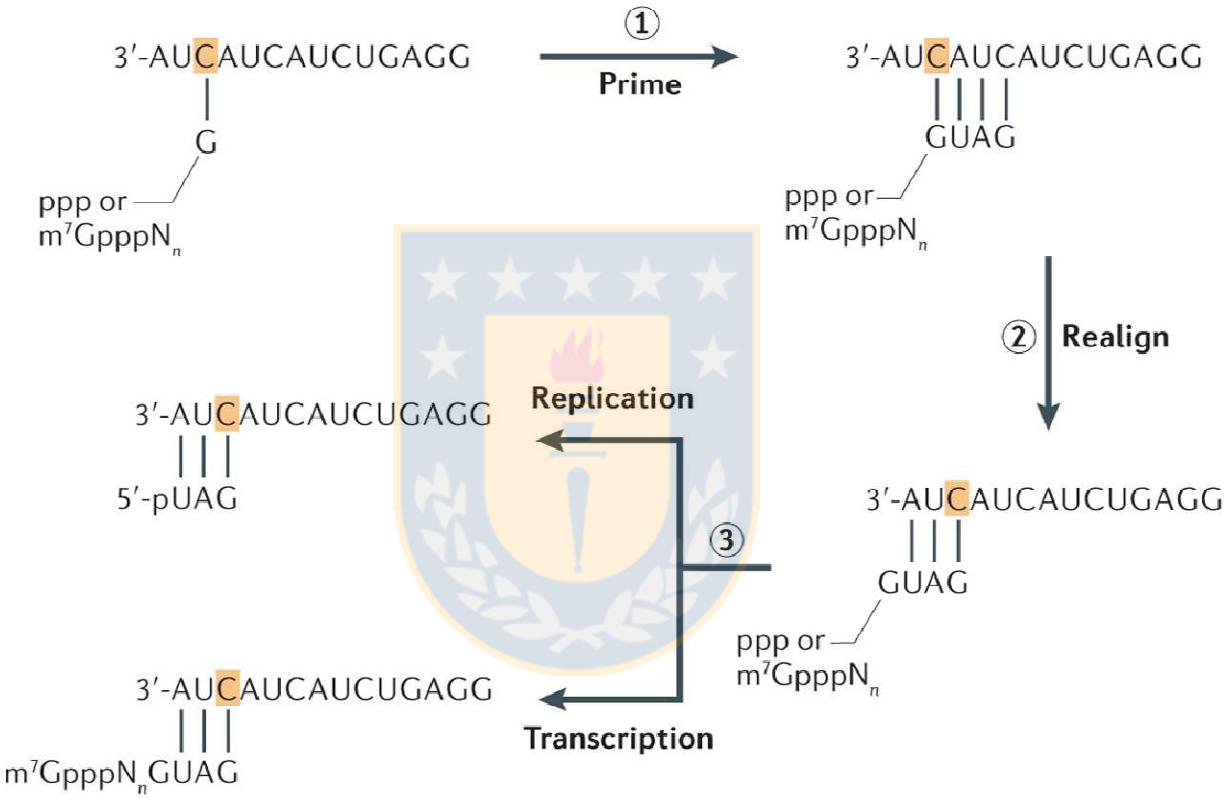

Fig.3. Prime-and-realign model for hantaviruses RNA synthesis initiation (Vaheri et al. 2013).

m^7Gppp structure added to the nascent mRNAs is recognized by the cells translational machinery, the ribosomal translocation disrupts any spurious transcription termination signal. Moreover, viral protein synthesis is stimulated by the interaction of the mRNA 5´-cap with their 3´ untranslated region (UTR) or poly(A) tail (Vera-Otarola et al. 2010; Hutchinson et al. 1996). Different nucleotide sequences and methods have been identified for each segment to be involved in the culmination of transcription (Hutchinson et al. 1996). The sequence motifs used for this intend are expected to form stem-loops critical to the dissociation of the L protein from the vRNA template. Accordingly, the generated mRNAs are naked and usually smaller than their respective vRNA.

The expression of viral proteins, specially increasing amounts of NP needed to coat the viral genome, might participate in the change from transcription to replication. This requires the L protein, either acting alone or in concert with undefined viral or cellular factors, to switch from primed to *de novo* mRNA synthesis (Reguera et al. 2016). During replication, the genome is processed to create complementary RNAs (cRNA) which are packaged and used as templates for the multiplication of the vRNAs. Shrouding of the vRNA and cRNA by NP can serve as an anti-termination signal, thus allowing the synthesis of full-length copies of the viral genome (Kaukinen et al. 2005). The presence of 5´-monophosphates on the genome and positive-sense antigenome intermediate suggests the usage of a nucleoside triphosphate (NTP), possibly GTP or ATP, to begin the reaction. It has been theorized that after realignment the overhanging nucleotides are removed by the same nucleolytic protein domain involved in "cap-snatching" (Garcin et al. 1995).

III. 3. L protein, a versatile molecular machine

The amino acids sequence analysis of proteins from members of the *Orthomyxoviridae*, *Bunyaviridae* and *Arenaviridae* families, all segmented negative-ssRNA viruses (sNSV), has shown a common RdRp domain. Under

physiological conditions, this domain catalysis the formation of phosphodiester bonds between ribonucleotides in an RNA template-dependent fashion. Thereby, being responsible for transcription and replication of their viral genomes.

ANDV exhibits the RdRp domain in the center of the L protein with the canonical closed right-hand-shaped architecture resembling the fingers, fingertips, palm and thumb (Kukkonen et al. 2005; van Dijk et al. 2004). The palm subdomain possesses sequence motifs A (973-DATKWS), B (1059-QGNLNKCSSL), C (1098-SDD), D (1154-GSIKVSPKKTT) and E (1171-EFLST). Whilst, fingertips and fingers subdomains include motifs F (885-KYQRTEADR) and G (628-RYLI) respectively (Fig.4.) (Gerlach et al. 2015). Motifs A and C are spatially juxtaposed and each contain an Asp residue, Asp973 and Asp1099, binding divalent cations involved in the creation of phosphodiester bonds by a two-metal ion mechanism. Together motifs A and B play key roles in the NTP selection via recognition of their 2´-hydroxyl group. Additionally, the flexible Gly1060 in motif B is important for post-catalysis translocation of the template-product duplex. Especially relevant for sNSVs is motif D, as it participates in the primer-dependent RNA synthesis of transcription (Castro et al. 2009). Meanwhile, motif E interacts with the backbone of the second and third nucleotide of the product RNA. One structural attribute that distinguishes most RdRp is their close hand conformation with well-defined template and NTP tunnels (van Dijk et al. 2004). Inference from the *La Crosse virus* (LACV; genus *Orthobunyavirus*, family *Bunyaviridae*) L protein structure lets to consider that when properly folded, motif F forms the roof of the NTP entry tunnel and motif G positions the priming NTP in the active site (Gerlach et al. 2015).

Except for the central RdRp domain, the rest of ANDV L protein is poorly characterized functionally and structurally. In spite of the sequence divergence, monomeric bunyavirus and heterotrimeric influenza polymerases have an evolutionary conserved architecture to match their similar mode of action

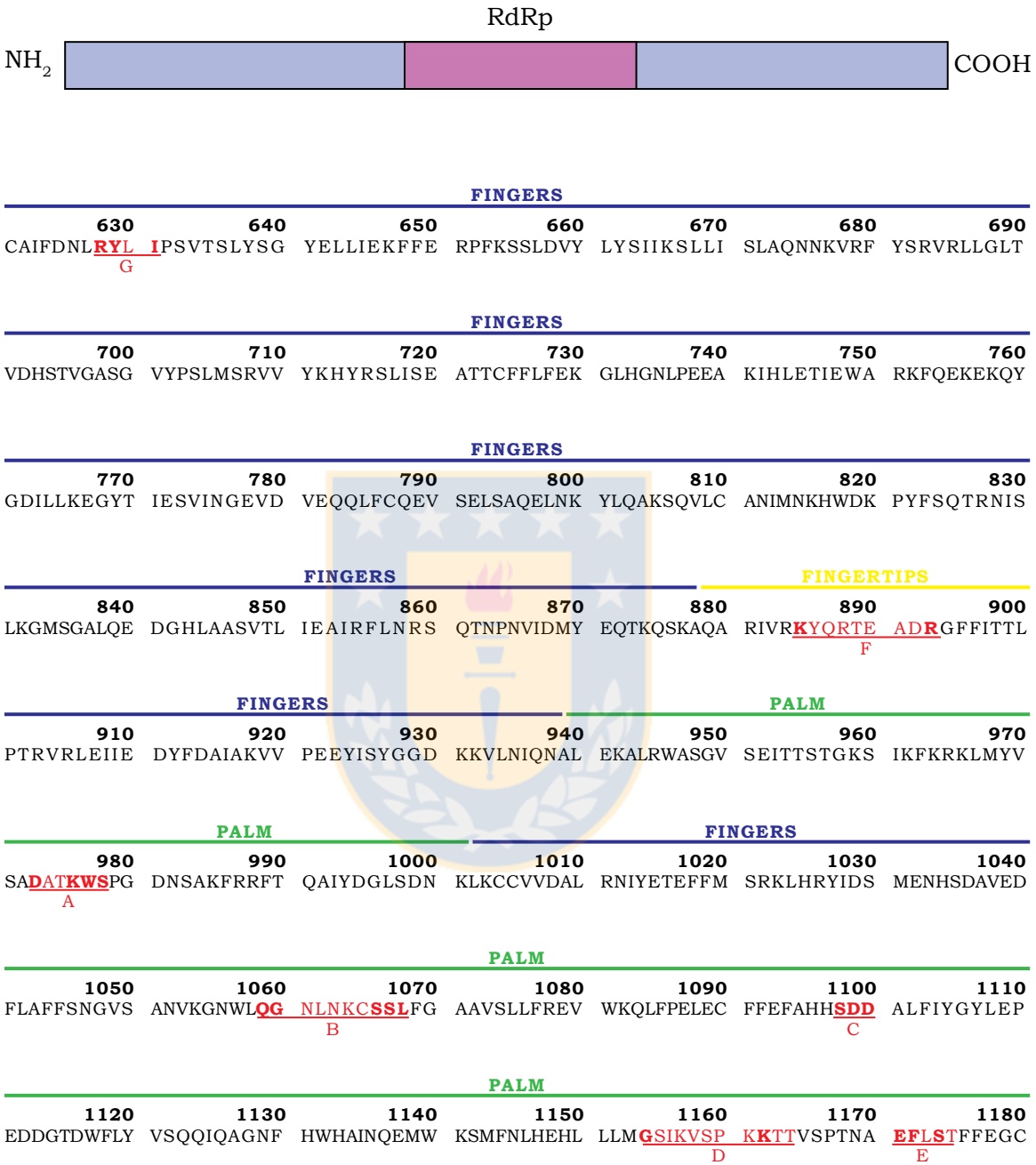

Fig.4. Illustration of the RdRp domain within ANDV L protein. Its amino acid sequence highlighting in red conserved motifs A-G and showing in bold residues present in all sNSVs. Displayed in different colors are the span of the putative structural subdomains of the fingers, fingertips and palm.

(Gerlach et al. 2015). In this manner, it is likely that the 2153 residues long ANDV molecule possesses additional enzymatic and regulatory activities as does the IFV PA-PB1-PB2 subunits complex. Recently, it has been reported the inhibitory effect of its N-terminal region on the viral and host-cell mRNA expression (Heinemann et al. 2013). An endonuclease domain, essential for viral cap-dependent transcription, has been identified at the N-terminus of the L protein for *Lymphocytic Choriomeningitis virus* (LCMV) and *Lassa virus* (LASV) both from the *Arenaviridae* family and for LACV from the *Bunyaviridae* family (Reguera et al. 2010; Morin et al. 2010; Wallat et al. 2014). Furthermore, a conserved PD…(E/D)…K nuclease motif is also found in the extreme amino region of ANDV L protein, although there is no evidence of its catalytic activity (Steczkiewicz et al. 2012; Heinemann et al. 2013). This functional homology holds a great potential, in terms of conservation and specificity, as a pharmacological target for the development of antivirals against ANDV. Thus, it becomes interesting to proof the existence of the putative endonuclease domain in ANDV L protein and elucidate its druggability based on structural signatures between sNSVs.

The experimental **hypothesis** of this work assumes that the N-terminus of ANDV L protein contains a structurally conserved endonuclease domain with a druggable active site. To test the hypothesis we propose the following main and specific objectives:

Main objective:

- Study the function, structure and utility as a therapeutic target of ANDV L protein N-terminal domain.

Specific objectives:

- Characterize the *in vitro* nuclease activity of ANDV L protein N-terminal domain.
- Determine the structure of ANDV L protein endonuclease domain.
- Evaluate the potential of ANDV L protein endonuclease domain as a pharmacological target.

IV. MATERIALS AND METHODS

IV. 1. Materials

IV. 1. 1. Bacterial strains

- DH5α (#C2987, New England Biolabs): chemically competent *E. coli* cells suitable for high efficiency transformation. Strain genotype [*fhuA2 Δ(argF-lacZ)U169 phoA glnV44 Φ80 Δ(lacZ)M15 gyrA96 recA1 relA1 endA1 thi-1 hsdR17*].
- BL21-Gold(DE3) (#230132, Agilent Technologies): chemically competent *E. coli* cells suitable for high-level expression of heterologous proteins under IPTG induction of T7 polymerase from *lacUV5* promoter. Strain genotype [BF^- *ompT hsdS*($r_B^- m_B^-$)*dcm*$^+$ Tet^r *gal* λ(DE3) *endA* Hte].

IV. 1. 2. Virus strains

- *Andes virus*, strain Chile-9717869 (#GCF_000850405.1, BNITM): isolate from *O. longicaudatus* trapped in Chile. Reproduces essential attributes of HCPS in the animal model *M. auratus*.

IV. 1. 3. Cell lines

- VeroE6 (#CRL-1586, ATCC): epithelial cell line from kidney tissue of *C. aethiops*.
- BHK-21 (#CCL-10, ATCC): fibroblast cell line from kidney tissue of *M. auratus*.
- HEK-293 (#CRL-1573, ATCC): epithelial cell line from embryonic kidney tissue of *H. sapiens*.

IV. 1. 4. Media

IV. 1. 4. 1. Bacterial culture media and supplements

- LB: nutritionally rich medium; tryptone 1% w/v, yeast extract 0.5% w/v, NaCl 1% w/v, pH 7.
- LB Agar: solid LB medium; tryptone 1% w/v, yeast extract 0.5% w/v, NaCl 1% w/v, agar 2% w/v, pH 7.
- SOC: transformation recovery medium; tryptone 2% w/v, yeast extract 0.5% w/v, NaCl 10mM, KCl 2.5mM, $MgCl_2$ 10mM, $MgSO_4$ 10mM, glucose 20mM, pH 7.
- Carbenicillin (#6344, CarlRoth): antibiotic belonging to the carboxypenicillin subgroup.

IV. 1. 4. 2. Cell culture media, supplements and reagents

- DMEM (#P04-03550, PAN): Dulbecco's Modified Eagle Medium for cells with high-energy demand.
- FBS "Gold" (#A15-151, PAA): Fetal Bovine Serum provides many non-defined growth promoting and survival enhancing factors to cells in culture.
- Sodium Pyruvate Solution (#S11-003, PAA): energy source in addition to glucose.
- MEM Non Essential Amino Acids (#M11-003, PAA): contributes to cell growth and viability.
- Penicillin-Streptomycin (#15140, Gibco): antibiotics combined action against gram -positive and -negative bacteria.
- Fungizone Antimycotic (#15290, ThermoFisher Scientific): formulation of amphotericin B with sodium deoxycholate.
- Trypsin-EDTA (#L11-660, PAA): UV inactivated cell dissociation solution.

IV. 1. 5. Plasmid vectors

- pOPIN-F: from the high-throughput pOPIN Vector Suite family. Allows In-Fusion cloning and protein expression in bacteria, insect and mammalian cells. Adds an N-terminal His-tag followed by the 3C protease cleavage sequence to the cloned molecules.
- pCITE-ANDV-L-HA: vector containing ANDV L protein cDNA.

IV. 1. 6. Proteins

IV. 1. 6. 1. Enzymes

- Restriction: *Kpn*I (#R0142), *Hind*III (#R0104) (New England Biolabs)
- Q_5 HF DNA polymerase (#M0491, New England Biolabs): thermostable DNA dependent DNA polymerase with 3' to 5' exonuclease activity, fused to processivity-enhancing Sso7d domain.
- Proteinase K (#P6556, Sigma-Aldrich): serine protease with broad substrate specificity.
- T4 PNK (#EK0031, ThermoFisher Scientific): T4 polynucleotidekinase catalyzes the transfer of the γ-PO_4 from ATP to the 5'-OH group of single and double -stranded DNAs and RNAs.
- HRV-3C protease (BNITM): in-house recombinant production of His-tagged cysteine protease which recognizes the cleavage site Leu-Glu-Val-Leu-Phe-Gln*Gly-Pro.

IV. 1. 6. 2. Antibodies

- Anti-NP-ANDV (BNITM): in-house rabbit antisera production against ANDV NP.
- Anti-Rabbit IgG (#111-035-003, Jackson ImmunoResearch): pAbs against rabbit IgG purified from goat antisera and conjugated to HRP.

IV. 1. 6. 3. Ribonuclease Inhibitors

- RNasin (#N251B, Promega): protein mix that inhibits RNase families A, B and C by noncovalent binding.

IV. 1. 6. 4. Molecular weight ladder

- PageRuler Prestained Protein Ladder (#26616, ThermoFisher Scientific): prestained mixture of 10 recombinant proteins ranging from 10-170 kDa.

IV. 1. 7. Radioactive isotope

- [γ-^{32}P]ATP (#SRP-301, Hartmann Analytic): considered a β particle according to its radioactive decay properties. Radioactive concentration 370MBq (10μCi/μl) at delivery.

IV. 1. 8. Protein crystallization screens

- JCSG Core Suite I (#130924, QIAGEN): high-hit crystallization conditions used in initial screening.
- JCSG Core Suite II (#130925, QIAGEN): high-hit crystallization conditions used in initial screening.
- JCSG Core Suite III (#130926, QIAGEN): high-hit crystallization conditions used in initial screening.
- JCSG Core Suite IV (#130927, QIAGEN): high-hit crystallization conditions used in initial screening.
- JBScreen Plus HTS (#CS-507L, Jena Bioscience): additive screen used in the optimization of preliminary crystallization conditions.

IV. 1. 9. Antivirals

- DPBA (#003-179-166, MolPort): chelating agent with inhibitory properties against influenza virus PA endonuclease domain.
- RBV (#196066, MP Biomedicals): a nucleoside antimetabolite drug that interferes with duplication of viral genetic material.

IV. 1. 10. Kits

- In-Fusion HD EcoDry Cloning Kit (#639691, Clontech): lyophilized reaction components for single-step directional cloning of one or more fragments of DNA into any vector.
- NucleoSpin Gel and PCR Clean-up Kit (#740609, Macherey-Nagel): silica-membrane mini spin columns for nucleic acid purification.
- NucleoSpin Plasmid Kit (#740588, Macherey-Nagel): silica-membrane mini spin columns for plasmid purification.

IV. 1. 11. Oligonucleotides

IV. 1. 11. 1. In-Fusion cloning of ANDV L constructs

DNA	pOPIN-F L F:	5' AAGTTCTGTTTCAGGGCCCGATGGAAAAGTATAGAGAGATTCA 3'
DNA	pOPIN-F L163 R:	5' ATGGTCTAGAAAGCTTTATGTTTTAACTGCAACCACTGAG 3'
DNA	pOPIN-F L191 R:	5' ATGGTCTAGAAAGCTTTATATATCAGCTTGGACTAGACGC 3'
DNA	pOPIN-F L194 R:	5' ATGGTCTAGAAAGCTTTAGACATAATTTATATCAGCTTGGACTAGAC 3'
DNA	pOPIN-F L197 R:	5' ATGGTCTAGAAAGCTTTAATGCTCTCTGACATAATTTATATCAGC 3'
DNA	pOPIN-F L200 R:	5' ATGGTCTAGAAAGCTTTACTTTATTAAATGCTCTCTGACATAA 3'
DNA	pOPIN-F L211 R:	5' ATGGTCTAGAAAGCTTTAAAACATTGCCTCCAAAGATGC 3'
DNA	pOPIN-F L214 R:	5' ATGGTCTAGAAAGCTTTACTTTAAGTTAAACATTGCCTCC 3'
DNA	pOPIN-F L228 R:	5' ATGGTCTAGAAAGCTTTAAGGGATGTTAAAGTATCTCAGTTTAG 3'

IV. 1. 11. 2. Sequencing of ANDV L constructs

DNA	pOPIN F:	5' GGATCGGACCGAAATTAATACG 3'
DNA	pOPIN R:	5' CATATGTCCTTCCGAGTGAGA 3'

IV. 1. 11. 3. Mutagenesis of ANDV L

DNA	Y32V F:	5' CTACTGGATAGGCTCGTCGCTGTCAGACATGACC 3'
DNA	Y32V R:	5' GGTCATGTCTGACAGCGACGAGCCTATCCAGTAG 3'
DNA	R35H F:	5' CTGGATAGGCTCTACGCTGTCCACCATGACCTGGTTGACC 3'
DNA	R35H R:	5' GGTCAACCAGGTCATGGTGGACAGCGTAGAGCCTATCCAG 3'
DNA	H36R F:	5' CTCTACGCTGTCAGACGTGACCTGGTTGACC 3'
DNA	H36R R:	5' GGTCAACCAGGTCACGTCTGACAGCGTAGAG 3'
DNA	D37A F:	5' CTACGCTGTCAGACATGCCCTGGTTGACCAGATG 3'
DNA	D37A R:	5' CATCTGGTCAACCAGGGCATGTCTGACAGCGTAG 3'
DNA	D40E F:	5' GACATGACCTGGTTGAGCAGATGATAAAAC 3'
DNA	D40E R:	5' GTTTTATCATCTGCTCAACCAGGTCATGTC 3'
DNA	I43A F:	5' GGTTGACCAGATGGCAAAACATGACTGGTCTG 3'
DNA	I43A R:	5' CAGACCAGTCATGTTTTGCCATCTGGTCAACC 3'
DNA	K44A F:	5' GACCTGGTTGACCAGATGATAGCACATGACTGGTCTG 3'
DNA	K44A R:	5' CAGACCAGTCATGTGCTATCATCTGGTCAACCAGGTC 3'
DNA	N50A F:	5' CATGACTGGTCTGATGCTAAAGATGTAGAAAGACC 3'
DNA	N50A R:	5' GGTCTTTCTACATCTTTAGCATCAGACCAGTCATG 3'
DNA	P96A F:	5' CTTTTTCCGAATGACAGCAGATAATTATAAAATTAC 3'
DNA	P96A R:	5' GTAATTTTATAATTATCTGCTGTCATTCGGAAAAAG 3'
DNA	D97A F:	5' CCGAATGACACCAGCTAATTATAAAATTACAGGTAACTTG 3'
DNA	D97A R:	5' CAAGTTACCTGTAATTTTATAATTAGCTGGTGTCATTCGG 3'
DNA	N98A F:	5' CCGAATGACACCAGATGCTTATAAAATTACAGG 3'
DNA	N98A R:	5' CCTGTAATTTTATAAGCATCTGGTGTCATTCGG 3'
DNA	E110A F:	5' GATTGAGTTTATTGCAGTGACTGTAACAGCTG 3'
DNA	E110A R:	5' CAGCTGTTACAGTCACTGCAATAAACTCAATC 3'
DNA	K124A F:	5' GAGGTATTAGGGAGGCGAAAATAAAGTATG 3'
DNA	K124A R:	5' CATACTTTATTTTCGCCTCCCTAATACCTC 3'
DNA	K127A F:	5' GGGAGAAGAAAATAGCGTATGAAGGAGGCCTC 3'
DNA	K127A R:	5' GAGGCCTCCTTCATACGCTATTTTCTTCTCCC 3'
DNA	N167A F:	5' CAGATGGATCAGCCATCTCGACTCAGTGGCCC 3'
DNA	N167A R:	5' GGGCCACTGAGTCGAGATGGCTGATCCATCTG 3'

IV. 1. 11. 4. Nuclease assay substrates

RNA	27 IVT:	5' GGGGAAUUGUGAGCGGAUAACAAUUCC 3'
RNA	27 polyA:	5' AAAAAAAAAAAAAAAAAAAAAAAAAA 3'
RNA	27+R:	5' GAUGAUGCUAUCACCGCGCUCGUCGUC 3'
RNA	27-R:	5' GACGACGAGCGCGGUGAUAGCAUCAUC 3'
RNA	40 IVT:	5' GGGGAAUUGUGAGCGGAUAACAAUUCCCCGGAGUUAAUCC 3'
RNA	40 polyA:	5' AAAAAAAAAAAAAAAAAAAAAAAAAAAAAAAAAAAAAA 3'
DNA	27+D:	5' GATGATGCTATCACCGCGCTCGTCGTC 3'
DNA	27-D:	5' GACGACGAGCGCGGTGATAGCATCATC 3'

IV. 2. Methods

IV. 2. 1. Generation of N-terminus variants for ANDV L protein

- **DNA constructs design, cloning and mutagenesis**

The extent of amino acids which make for the N-terminal domain of ANDV L protein (NP_604473.1) was evaluated via a structure based multiple sequence alignment with human pathogenic hantaviruses SNV (NP_941976.1), HNTV (NP_941982.1) and TULV (NP_942124.1) using their homologous LACV (NP_671968.1) resolved atom structure (PBD ID: X2I5) as reference model. Such analysis were performed with Clustal Omega (McWilliam et al. 2013), Jpred4 (Drozdetskiy et al. 2015) and ESPript 3 (Robert & Gouet 2014) bioinformatic softwares.

The cDNA of fragments encoding residues 1- 163, 191, 194, 197, 200, 211, 214 and 228 from the L protein of ANDV strain Chile 9717869 were amplified by PCR employing the pCITE-ANDV-L-HA plasmid as a template. The amplification reactions were carried out in a final volume of 25µl with 10ng of plasmid, 0.5pmols of each corresponding oligo, 50pmols of each dNTP, 1X Q_5 buffer and 0.5U of Q_5 HF DNA polymerase. Set of reactions were prepared simultaneously with a negative control lacking the plasmid DNA. The thermal cycling program consisted of an initial 30s denaturation step at 98°C followed by 35 cycles of 30s denaturation at 98°C – 30s annealing at 58°C – 30s extension at 72°C and a final extension at 72°C for 2min. PCR products were purified from 1% agarose gels utilizing the NucleoSpin Gel and PCR Clean-up Kit and cloned into *Kpn*I/*Hind*III linearized pOPIN-F with the In-Fusion HD EcoDry Cloning Kit. Half of the In-Fusion reaction was used to transform DH5α cells by incubations for 45s at 42°C and 2min on ice followed with 1h of recovery in SOC media at 37°C. Plasmid DNA was purified via NucleoSpin Plasmid Kit from colonies

grown under antibiotic selective pressure. The integrity of all constructs was confirmed by sequencing.

Single amino acid mutants (Y32V, R35H, H36R, D37A, D40E, I43A, K44A, N50A, P96A, D97E, N98A, E110A, K124A, K127A and N167A) were created by two-step PCR mutagenesis. The first step included the separate amplification of two fragments with an overlapping region comprising the desired mutagenic site. One reaction used oligonucleotides complementary to the 5´-end of the coding sequence and the desired mutagenic site with introduced changes. The other reaction used oligonucleotides complementary to the same desired mutagenic site with the corresponding changes and the 3´-end of the coding sequence. The second step used the purified PCR products from the previous reactions as overlapping templates together with the primers for the 5´ and 3´ -ends of the coding sequence for the new amplification reaction. The resulting fragments were cloned into pOPIN-F as mentioned before. The PCR mixes were prepared as described above and always used the same cycling program.

- **Protein test-expression**

To assess the soluble expression of the recombinant variants, BL21-Gold(DE3) cells were transformed with 100ng of the respective DNA construct and seeded in 5ml LB media supplemented with 100µg/ml carbenicillin. Mini cultures were incubated overnight at 37°C with agitation. The samples which grew were reseeded under the same conditions until they reached an OD_{600} between 0.6-0.9, at this point IPTG was added to a final concentration of 0.5µM and the cells were incubated overnight at 17°C. Subsequently, the cells were centrifuged for 5min at 5000g and 4°C. Cell pellets were resuspended in 1ml of ice cold Lysis buffer (50mM Tris-HCl pH 7.4, 300mM NaCl, 10mM imidazole, 10% (v/v) glycerol and fresh 1mM PMSF) and sonicated maintaining the temperature under 10°C. The insoluble and soluble fractions were separated by

centrifugation for 30min at 12000g and 4°C. The pellets were resuspended in 1ml of Lysis buffer. Soluble fractions were incubated for 1min on ice with 50µl of 50% slurry Ni-NTA agarose beads (#30250, QIAGEN), centrifuged for 2min at 700g and 4°C and washed 3 times with Lysis buffer. Samples corresponding to the insoluble, soluble and bead-bound fractions were evaluated through one-dimensional SDS-PAGE.

- **Protein production**

Overnight cultures of transformed BL21-Gold(DE3) cells with pOPIN-F-ANDV L_{200} mutants were used to inoculate 1L LB media supplemented with 100µg/ml carbenicillin. These cultures were incubated at 37°C with agitation until they reached an OD_{600} between 0.6-0.9, at this point the flasks were transferred to ice cold water to lower their temperature and the recombinant expression of proteins was induced overnight at 17°C by adding IPTG to a final concentration of 0.5µM. Afterwards the media were centrifuged for 30min at 5000g and 4°C. Cell pellets were resuspended in 50ml of ice cold Lysis buffer containing 10mM $MnCl_2$, disrupted by sonication on ice and centrifuged for 30min at 12000g and 4°C. The soluble fraction was applied onto a Ni-NTA agarose column, which was washed with 10 column volumes of Wash buffer (50mM Tris-HCl pH 7.4, 1000mM NaCl, 50mM imidazole and 10% (v/v) glycerol) and eluted with 5 column volumes of Elution buffer (50mM Tris-HCl pH 7.4, 1000mM NaCl, 250mM imidazole and 10% (v/v) glycerol). For crystallization setups, the N-terminal tag of ANDV L_{200} K127A was removed by an overnight incubation at 4°C with HRV-3C protease using a 1:10 ratio in 10ml of Cleavage buffer (50mM Tris-HCl pH 7.4, 1000mM NaCl, 5% (v/v) glycerol and 2mM DTT) as it dialyzed against this same buffer to reduce the imidazole concentration carried over from the previous elution of the affinity chromatography. Proteins were further purified by size exclusion chromatography using a HiLoad 16/600 Superdex 200 column (#28989335, GE Healthcare Life Sciences) in ANDV L_{200} buffer

(50mM sodium citrate pH 5.5, 1000mM NaCl and 5% glycerol) at 4°C. All eluted fractions were assessed by one-dimensional SDS-PAGE, concentrated up to 1mg/ml or 10mg/ml using Amicon Ultra-4 with 10kDa cut off (#UCF-801024, Millipore), flash frozen in liquid nitrogen and stored at -20°C.

IV. 2. 2. One-dimensional SDS-PAGE

The protein samples and the molecular weight ladder were mixed with appropriate volumes of 4X loading buffer (200mM Tris-HCl pH 6.8, 400mM DTT, 8% SDS, 0.4% bromophenol blue and 40% glycerol) and heated at 95°C for 5min. Subsequently, they were loaded onto 12 or 16 % polyacrylamide gels and separated under reducing and denaturing conditions. The gels were run at 100-150 V for 1h in 1X Tris-Glycine buffer (25mM Tris-HCl pH 8.3, 250mM glycine and 0.1% SDS). Inspection of the separated proteins was accomplished by staining with Coomassie Blue solution (0.5g/L Coomassie Brilliant Blue R-250, 50% (v/v) methanol and 10% (v/v) HAc) for 30min at room temperature followed by at least a 30min incubation in Destain solution (50% (v/v) methanol and 10% (v/v) HAc).

IV. 2. 3. Bacterial growth kinetics

The effect of the heterologous expression of ANDV L_{200} mutants on the growth of BL21-Gold(DE3) cells was evaluated in accordance to their generation time. Equal amounts of transformed cells to obtain an OD_{600} of 0.05 were seeded in 50ml LB media supplemented with 100µg/ml carbenicillin and incubated at 37°C with constant agitation. The OD_{600} of all cultures was measured every 30min and their growth curves were constructed by plotting the logarithm of the absorbance of cultures at 600nm against time. To compute the doubling time expressed in minutes, within the phase of exponential growth, Δt (the time

difference) between q2 (OD_{600} at t_2) and q1 (OD_{600} at t_1) was multiplied by the fraction of log2/log (q2/q1) as shown in the equation below.

$$min = \Delta t \frac{log2}{log \frac{q2}{q1}}$$

IV. 2. 4. Thermal shift assays

The effect of different solution components on the stability of ANDV L_{200} variants was determined through a thermofluor-based method (Ericsson et al. 2006). In all cases, the 25µl reaction mixtures containing 10µM of protein, 1X Sypro Orange (#S6650, Invitrogen) and tests buffers were set in 96 well PCR plates. Fluorescence changes, within wavelengths of excitation of 490nm and emission of 575nm, were monitored for 0.2°C increments in temperatures ranging from 20 to 90 °C using a real-time PCR instrument. The analysis of the data was achieved by comparing the Tm values measured from the samples with their respective controls where water was added to the reaction mixture instead of the test buffer compound.

The optimization of buffer elements to improve protein sample stability and solubility during large scale purification and further crystallization setups involved the use of ANDV L_{200} mutant K44A. Buffer screens consisted of an array of 7 different acid-base pairs with a pH spectrum from 5 to 9 (sodium citrate, MES, sodium phosphate, HEPES, Tris, imidazole and bicine) each at a concentration of 100mM, ionic strengths ranging from 0 to 1M of NaCl and 13 additives each at a 5mM final concentration (β-octylglucoside, ZnAc, CaAc, MgAc, $MnSO_4$, glycerol, glucose, DTT, TCEP, PEG1000, ATP, GTP and UTP).

The impact of single residue mutations on ANDV L_{200} stability and ability to bind ligands such as divalent ions or DPBA was evaluated in 50mM Tris-HCl

pH 7.2, 250mM NaCl and 5% glycerol complemented with either 10mM EDTA, 4 or 16 mM $MgCl_2$ and 4 or 16 mM $MnCl_2$ in the presence or absence of 25µM DPBA.

IV. 2. 5. Nuclease activity assays

In order to identify and characterize the nuclease activity of ANDV L_{200}, its mutants were incubated with various ^{32}P-labeled oligonucleotides as substrates and the outcomes of the reactions were analyzed via urea-polyacrylamide gel electrophoresis.

All reagents and plasticware used were certified to be DNase-RNase free. Non-disposable glassware was treated overnight with 0.1% (v/v) DEPC water at 37°C and then autoclaved for 15min at 125°C. Meanwhile, electrophoresis tanks were cleaned with 0.5% (w/v) SDS, rinsed with RNase-free water and allowed to dry.

- **Radioactive labeling and hybridization of substrates**

The synthesized oligonucleotides were resuspended up to 500µM for stocks and 100µM for working solutions in RNase-free water containing 0.25U/µl RNasin. The 5´-ends of 100pmols for each oligo were radioactively labeled by 10U of T4 PNK which catalyzed the γ-PO_4 transfer from 20µCi [γ-^{32}P]ATP in a 20µl reaction mix containing 50mM Tris-HCl pH 7.6, 10mM $MgCl_2$, 5mM DTT, 0.1mM spermidine and 0.25U/µl RNasin. After 1h at 37°C, the unincorporated [γ-^{32}P]ATP was removed using Illustra MicroSpin G25 columns (#27-5325-01, GE Healthcare Life Sciences) and the labeled substrates were stored at 4°C for up to 1 month.

Double-stranded RNA and DNA substrates were generated by hybridization of complementary sequences present in RNA (27+R and 27-R) and DNA (27+D and

27-D) oligonucleotides. Equal amounts of each complementary oligo, where one of them was radioactively labeled, were mixed and heated for 5min at 98°C in a standard thermoblock which was subsequently turned off. The hybridization process was promoted through a slow cooling down overnight period after which the resulting probes were stored until usage.

- **Nuclease activity of ANDV L_{200}**

To ascertain the nuclease activity of ANDV L_{200} and the role of specific amino acids on its enzymatic function, 1µM of the respective mutant was incubated with 0.1µM ^{32}P-labeled RNA 27 IVT oligonucleotide in 50mM Tris-HCl pH 7.2, 250mM NaCl, 5% glycerol and 0.25U/µl RNasin in the presence or absence of 2mM $MnCl_2$ at 37°C for 1 and 2 h. The 20µl reactions were stopped by addition of an equivalent volume of 2X loading buffer (95% formamide, 18mM EDTA, 0.025% SDS, xylene cyanol and bromophenol blue) and heating for 5min at 98°C followed by 5min on ice.

Under the same assay conditions, ANDV L_{200} mutants K44A, D97E and N167A were used to evaluate the impact of substrates accessibility and length on their nuclease activity by comparing the percentage of degradation of structured (RNA 27 IVT or RNA 40 IVT) versus unstructured (RNA 27 polyA or RNA 40 polyA) radiolabeled oligonucleotides. Likewise, to examine the spectrum of nucleic acid species cleaved by ANDV L_{200}, single and double-stranded RNA (27+R and 27+R:27-R, respectively) and DNA (27+D and 27+D:27-D, respectively) substrates were used.

Furthermore, the metal ion specificity of a set of ANDV L_{200} mutants was assessed using the labeled RNA 27 polyA probe in the buffer mentioned above with or without 2mM of $MgCl_2$ or $MnCl_2$.

A time course analysis of the reaction was made for ANDV L_{200} N167A employing either RNA 27 IVT or RNA 27 polyA as substrates. Additionally, the effect of increasing amounts of DPBA on the enzymatic activity of the formerly mentioned mutant was established by a 15min preincubation at room temperature of the reaction components before the addition of the labeled RNA 27 IVT probe.

- **Urea-Polyacrylamide gel electrophoresis**

The reactions products were separated by electrophoresis in denaturing urea-polyacrylamide gels (8M urea, 20% polyacrylamide, 90mM Tris-HCl, 90mM Borate, 2mM EDTA, 0.1% APS and 0.1% TEMED) polymerized in disposable casts (#MW2010, Invitrogen). The gels were pre-run at 180V for 30min in 1X TBE (90mM Tris-HCl, 90mM Borate and 2mM EDTA) before the samples were added, after which the gels were run for an additional 60min. For visualization, the gels were exposed to a Storage Phosphor Screen (#28-9564-74, GE Healthcare Life Sciences) for 1h at 4°C and resulting images were digitalized using a Typhoon scanner. Further analysis and quantification of the signals intensities was made with ImageJ software (Schneider et al. 2012).

IV. 2. 6. Limited proteolysis

A fix amount of 1mg of ANDV L_{200} K44A was incubated for 1h at room temperature with increasing concentrations of proteinase K (0.005µg/µl, 0.05µg/µl, 0.5µg/µl and 5µg/µl) in 50µl of Elution buffer. A negative control of the reaction was carried out in the absence of the enzyme. The digestion products were evaluated by one-dimensional SDS-PAGE.

IV. 2. 7. Crystallization

Initial crystallization conditions were examined by the sitting-drop vapor-diffusion method using JCSG Core Suite I, II, III, IV and JBScreen Plus HTS commercial screens. At room temperature, 10mg/ml of ANDV L variant K127A harboring the first 200, 211, 214 and 228 amino acids were seeded manually in a 1:1 ratio with the respective reservoir solution. The resulted 2µl sample drops were equilibrated against 250µl of reservoirs and monitored for the appearance of crystals for up to 2 weeks. Discrimination between salt and protein crystals was achieved by 0.05% (w/v) methylene blue staining.

Optimization of the protein crystals was done by seeding different concentrations (5, 7.5 and 10 mg/ml) of ANDV L_{200} K127A in gradient-based solution matrices made up of the most frequent pH acid-base pairs, precipitants and additives found in the initial crystallization hit solutions. Further improvements were assessed at 4 and 22 °C using 1:1, 1:2 or 1:3 sample to reservoir ratios by the sitting or hanging–drop vapor-diffusion method.

Selected crystals were harvested, soaked for 1min in its reservoir solution supplemented with either 8% (v/v) 2,3-butanediol or 20% (v/v) glycerol as cryoprotectant and flash frozen in liquid nitrogen.

IV. 2. 8. X-ray data collection and structure determination

Diffraction data were collected at beamline ID23-1 of the European Synchrotron Radiation Facility in Grenoble-France, with wavelengths of 0.98 and 1.77 Å for native and anomalous information respectively. Datasets were processed with iMosflm (Battye et al. 2011) and experimental phases were obtained by molecular replacement with HNTV endonuclease (PDB ID: submitted) as search model using PHASER software (McCoy et al. 2007). Models were manually build

into the electron density maps with Coot (Emsley et al. 2010) and refined by iterative cycles with PHENIX (Adams et al. 2010). Meanwhile, the electrostatic potential maps were calculated using PDB2PQR and APBS (Dolinsky et al. 2007; Baker et al. 2001). Structural figures were created with PyMOL (DeLano 2002). Finally, the atomic coordinates of ANDV L_{200} K127A were deposited in the PDB (PBD ID: 5HSB).

IV. 2. 9. Cell lines culture

Unless otherwise specified, all cell lines were grown in complete media (DMEM supplemented with 10% FBS, 1mM sodium pyruvate, 1X MEM Non Essential Amino acids, 1X Penicillin-Streptomycin and 1X Fungizone) with incubation at 37°C under a humidified atmosphere containing 5% CO_2. Sub-confluent maintenance of the cell lines was achieved by consecutive 1:10 dilutions of 0.25% Trypsin-EDTA treated monolayers.

IV. 2. 10. ANDV stock production

ANDV was propagated in VeroE6 cells using newly prepared viral inoculums at a MOI of 0.1 in infection media (DMEM supplemented with 2% FBS, 1mM sodium pyruvate, 1X MEM Non Essential Amino acids, 1X Penicillin-Streptomycin and 1X Fungizone). Inoculums were incubated during 1h with 50% confluent monolayers of cells, after which the media was refreshed. Supernatants were collected 7 days post-infection, filtered through a 0.2µm pore membrane (#SLFG025LS, EMD Millipore), divided into aliquots and stored at -80°C until usage. Stocks titers varied between batches from 10^4-10^6 FFU/ml.

IV. 2. 11. Virus titration

Viral titers in supernatants of infected cells were determined by focus-forming assays. VeroE6 cells were seeded into 24 well plates at a density to achieve 80% confluency by the following day. Starting from frozen samples, 10 fold serial dilutions reaching up to 10^{-5} were prepared in infection media. Complete media from the 24 well plates was removed, cells were washed with infection media and 200µl of each dilution or infection media as negative control was added per well. Following 1h incubation, the inoculums were removed and the cells were washed with infection media before addition of 2ml per well of overlay media (infection media supplemented with 1% methylcellulose (#M0262, Sigma-Aldrich)). Plates were then incubated for 10 days, after which the overlay media was removed and cells were fixed with 4% formaldehyde for 25 min at RT. During fixation virus particles were inactivated and the rest of the procedure was carried out under biosafety level 2 (BSL-2) lab conditions. Cells were washed 3 times with 1X PBS (10mM Na_2HPO_4, 1.8mM KH_2PO_4, 137mM NaCl, 2.7mM KCl), permeabilized with 0.5% Triton X-100 for 30 min and blocked with 10% FBS in 1X PBS for 1h at RT. Afterwards, cells were covered by a 1:1000 dilution of anti-NP-ANDV antibody for 1h at RT followed by 3 washing steps with 1X PBS and later incubation for another hour at RT with 1:2500 dilution of HRP conjugated anti-Rabbit IgG antibody. Finally, infected cells were stained after thoughtful washing with 1X PBS by 20 min incubation in the dark with TMB solution (#10008, Mikrogen). To calculate the viral titers expressed as FFU/ml (focus-forming units per ml), F (the number of foci ≥ 20 in the well for the highest serial dilution) was divided by the Fd (dilution factor) and the Vi (inoculum volume) as shown in the equation below.

$$FFU/ml = \frac{F}{(Fd)(Vi)}$$

IV. 2. 12. Viral growth kinetic

Cell lines VeroE6, BHK-21 and HEK-293 were seeded into 24 well plates at a density to obtain 50% confluency by the following day. At this point, fresh viral inoculums in infection media at a MOI of 0.5 were added to the cells monolayers and incubated for 1h at 37°C. After the removal of the inoculums, the cells were washed with 1X PBS and were left in 1ml per well of infection media. The supernatants from two wells were harvested every 24h for 11 days, centrifuged at 150g for 5min at room temperature and stored at -80°C until later virus titration.

IV. 2. 13. *In vitro* antiviral activity and cytotoxicity

Monolayers of 80% confluent VeroE6 cells were inoculated with ANDV at a MOI of 0.5. After 1h incubation, the inoculums were replaced by 1ml per well of treatment media (infection media supplemented with either DPBA or RBV to obtain working concentrations of 500µM, 250µM, 50µM, 25µM, 5µM, 0.5µM and 0µM as negative control). Stocks of 100mM DPBA and RBV were prepared in 50% DMSO and 1X PBS, respectively. Treatment media was carefully made to maintain constant amounts of stock solvents, where DMSO did not exceeded 0.25%. Virus titers in supernatants collected 3 days followed infection were determined from triplicates of samples for each antiviral working concentration. Compounds concentrations that reduced infectious virus titers by 50% (IC_{50}), 90% (IC_{90}) and 99% (IC_{99}) were calculated from dose-response curves using GraphPad Prism 6.0 software.

In parallel, mock infected cells were used to determine the cytotoxicity effect of each compound concentration via an MTT assay. After collection of the supernatants, the monolayers of cells were incubated for 90min at 37°C with infection media containing 1mg/ml of MTT (#135038, Sigma). The blue

formazan crystals formed were dissolved in isopropanol and 100µl of the resuspensions were transferred to a 96 well plate. Cell viability was assessed by the measured absorbance at 550nm blanked to the background at 630nm and normalized against their respective negative control.

Remarks: ANDV handling was strictly performed in high containment biosafety level 3 (BSL-3) facilities at the Bernhard Nocht Institute for Tropical Medicine (BNITM)-Germany.

V. RESULTS

V. 1. Characterize the *in vitro* nuclease activity of ANDV L protein N-terminal domain

V. 1. 1. Identify the amino acid sequence composition of ANDV L protein N-terminal domain

The amino acid sequence of ANDV L protein N-terminal domain constructs were selected via the structure based sequence alignment of human pathogenic hantaviruses using their homologous LACV resolved atomic structure (PDB ID: X2I5) as template (Fig.5.A). Oligos were designed for PCR amplification, from plasmid pCITE-ANDV-L-HA (kindly provided by Dr. Patrick Heinemann), of the nucleotide sequences encoding the first 163, 200 and 228 residues of the L protein and further In-Fusion cloning into the expression vector pOPIN-F. Due to the reports on the difficulties in the detection of the expression of the wild-type (wt) L protein, mutant K44A was generated for all variants in parallel (Fig.5.B). This mutation along with 14 others has been described to enhance the expression levels of the L protein in mammalian cells (Heinemann et al. 2013). The correct nucleotide sequence for every clone and mutant was confirmed by sequencing.

During the expression tests of ANDV L_{163}, L_{200}, L_{228} and their K44A version, there was no cell growth of transformed *E. coli* strain BL21-Gold (DE3) with pOPIN-F-ANDV- L_{200} and L_{228}. Expressed ANDV L_{163} and L_{163} K44A were detected in the insoluble fraction of bacteria. Meanwhile, the expression of soluble proteins was detected for ANDV L_{200} K44A and L_{228} K44A.The solvent exposure of the plasmid incorporated N-terminal His-tag was confirmed for both soluble alternatives since they were also observed in the Ni-NTA bead bound fraction (Fig.6). In all the cases, SDS-PAGE migration of the heterologous proteins corresponded to the expected molecular weight as

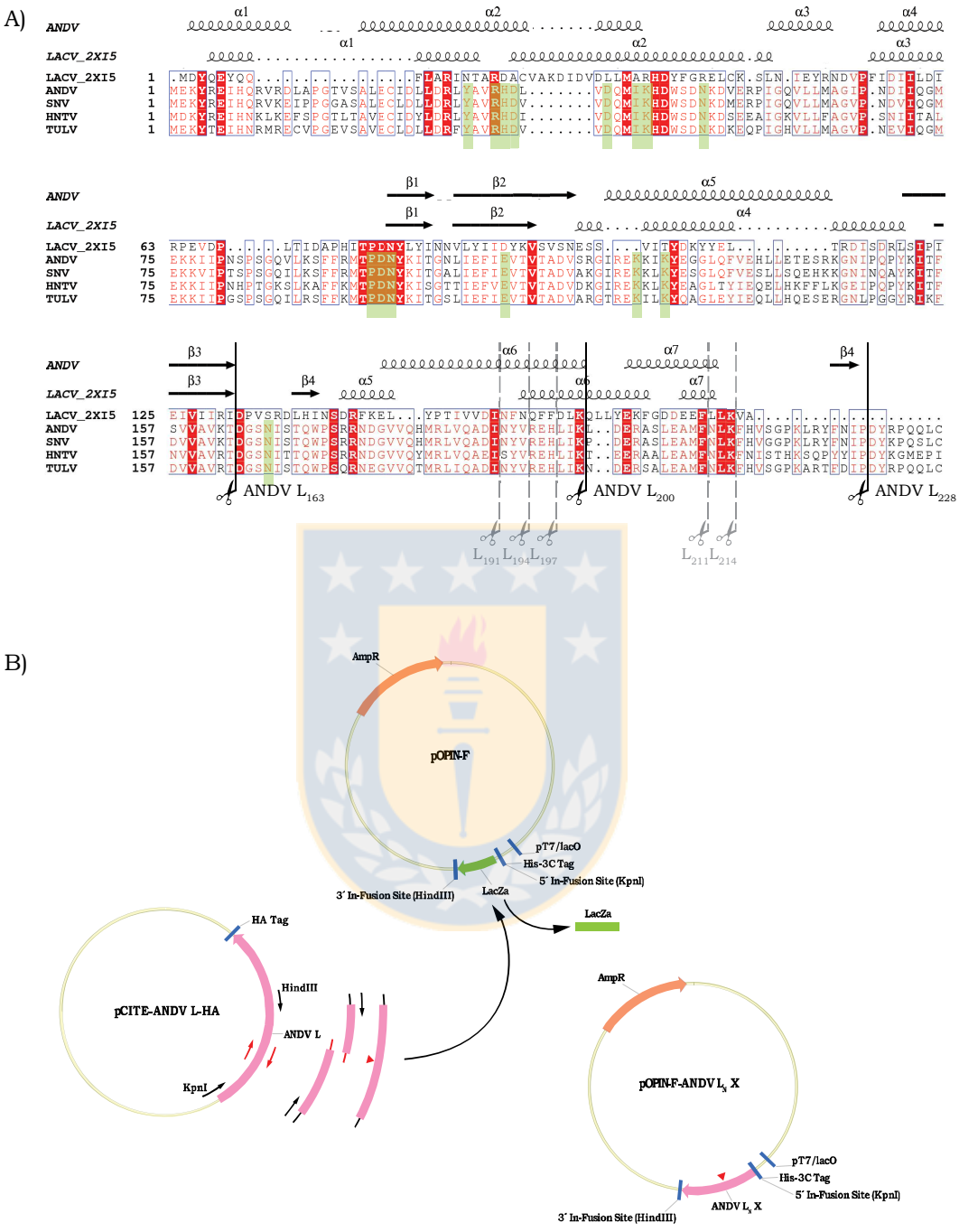

Fig.5. Design strategy for the generation of expression vectors for N-terminus variants of ANDV L protein. A) Structure based multiple sequence alignment of the L protein N-terminal region of ANDV, SNV, HNTV and TULV using the homologous atomic structure of LACV (PDB ID: X2I5) as template. The predicted and annotated secondary structures respectively for ANDV and LACV are shown above the alignment. Selected constructs are delimited by scissors and target residues for mutagenesis are highlighted in green. B) Schematic representation of the In-Fusion cloning and two-step PCR mutagenesis approach.

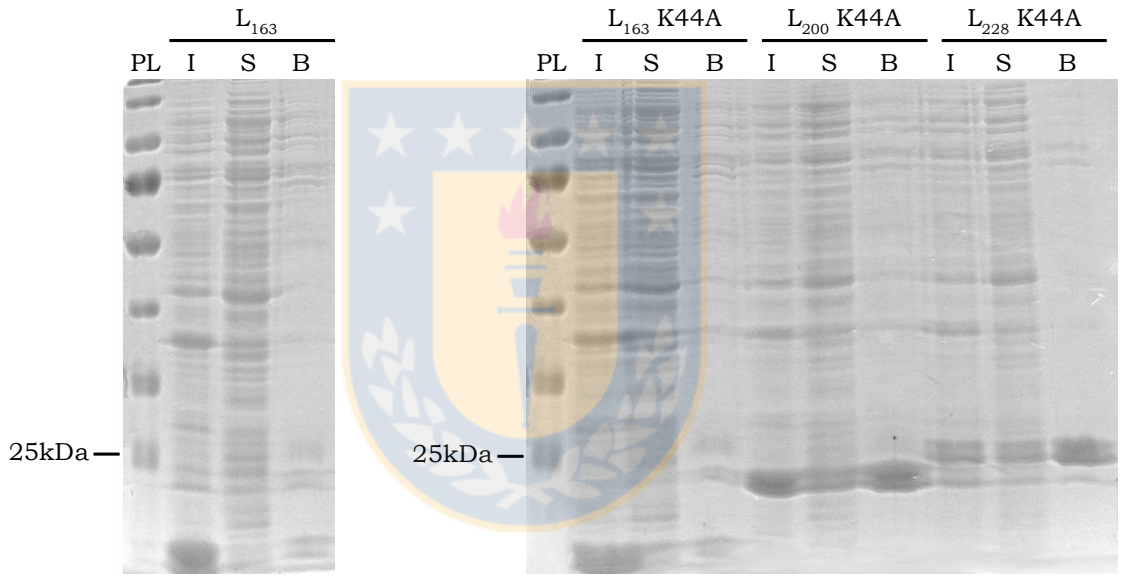

Fig.6. Evaluation of the effect of ANDV L protein N-terminal region on bacteria. Comassie blue staining of 12% SDS-PAGE for the analysis of the expression of constructs ANDV L_{163}, L_{200} and L_{228} of wt and K44A mutant sequences. Lanes PL: protein ladder, I: insoluble fraction, S: soluble fraction, B: Ni-NTA bead bound fraction.

compared to the protein ladder.

To recognize the minimal stable fragment that is well expressed and soluble, additional constructs were created for the L protein K44A mutant containing the first 191, 194, 197, 211 and 214 residues (Fig.5.A). The expression tests for all the variants mentioned above showed the initial 200 amino acids to be necessary for solubility while the recombinant protein levels do not vary significantly (Fig.7).

V. 1. 2. Production of ANDV L_{200}

Similar to the undetectable expression of ANDV full-length L wt protein in mammalian cells, it was impossible to obtain any of its N-terminal versions in a soluble form in bacteria. However, their K44A mutants were expressed at high levels and did not perturb *E. coli* cells viability (Fig.6 and 7).In order to assess mutations Y32V, R35H, H36R, D37A, D40E, I43A, K44A, N50A, P96A, D97E, N98A, E110A, K124A, K127A and N167A in the context of the N-terminal domain, these single amino acid alterations were incorporated into ANDV L_{200} (Fig.5).

The transformed BL21-Gold (DE3) cells with pOPIN-F-ANDV-L_{200} Y32V or D37A mimicked the wt phenotype where no bacterial growth was observed. Additionally, the generation times of *E. coli* populations without heterologous protein induction varied for the remaining 13 mutants from 32-41 min (Fig.8.A). Although there were differences in the expression levels of ANDV L_{200} mutants, these did not correlate with their corresponding doubling times (Fig.8.B).

To biochemically establish the nuclease activity of ANDV L protein N-terminal domain highly pure and correctly folded samples were required. The solution components to use throughout the purification process of ANDV L_{200} mutants

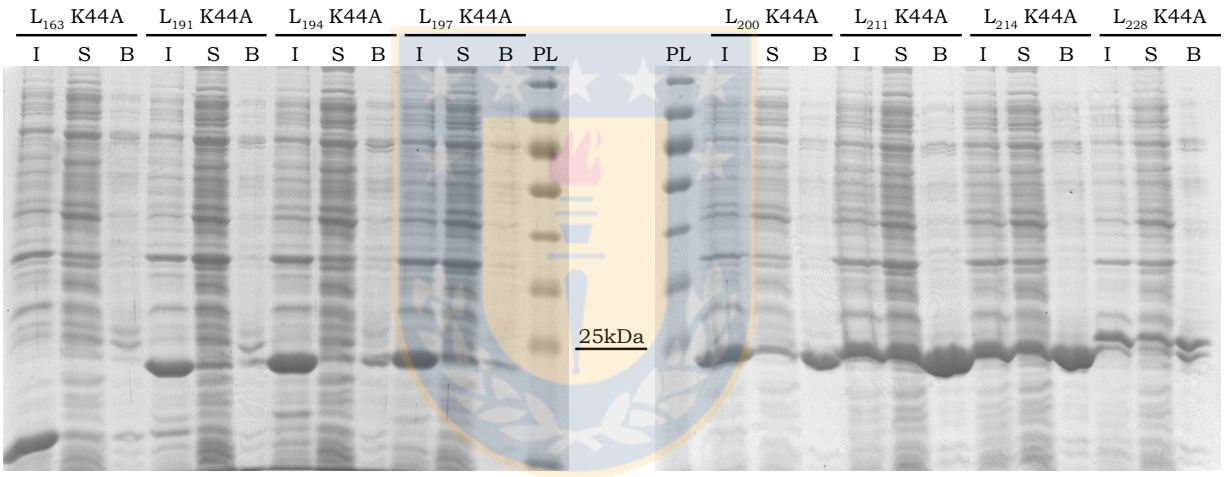

Fig.7. Examination of the amino acid sequence composition of ANDV L protein N-terminal domain. Coomassie blue staining of 12% SDS-PAGE for the analysis of the expression of constructs ANDV L_{163}, L_{191}, L_{194},L_{197}, L_{200},L_{211}, L_{214} and L_{228}K44A mutant sequences. Lanes PL: protein ladder, I: insoluble fraction, S: soluble fraction, B: Ni-NTA bead bound fraction.

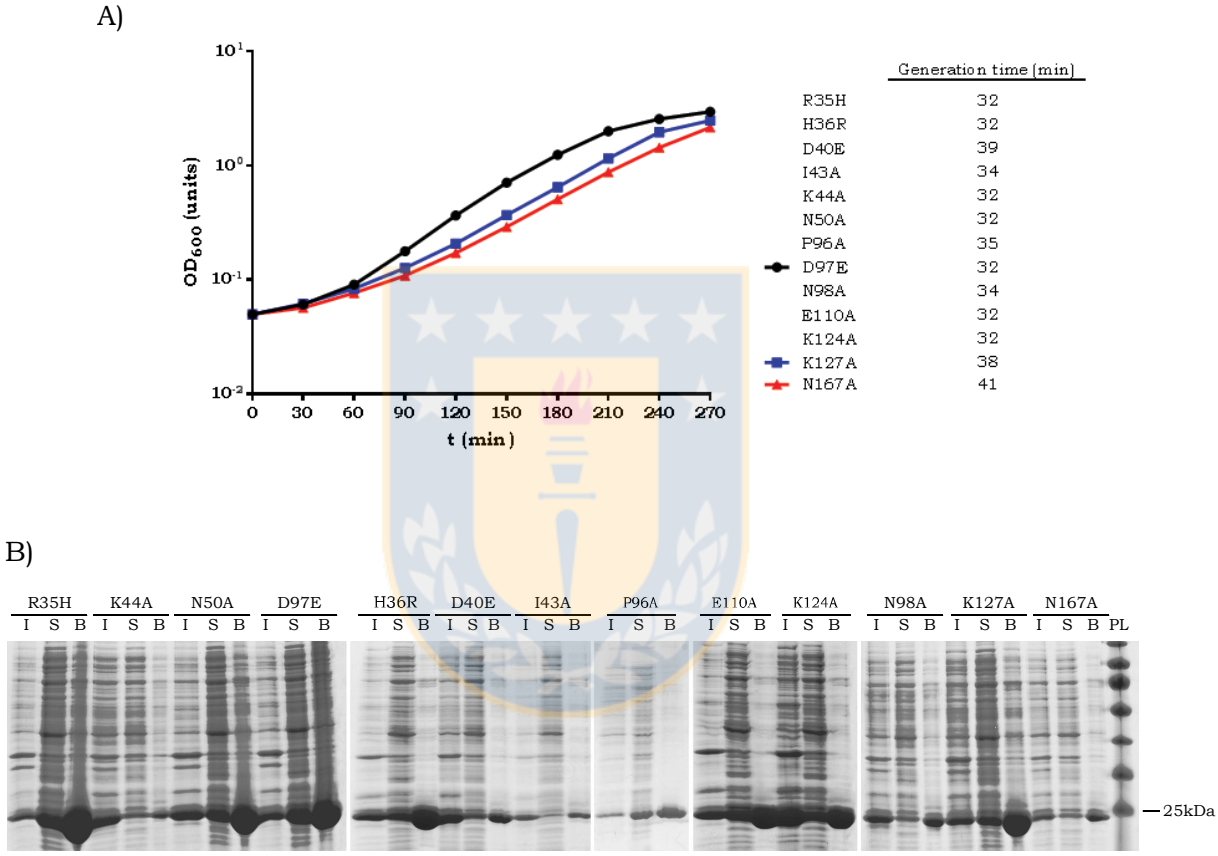

Fig.8. Evaluation of the effect of ANDV L_{200} single residue mutations on A) Bacterial viability and B) Recombinant protein expression. Lanes PL: protein ladder, I: insoluble fraction, S: soluble fraction, B: Ni-NTA bead bound fraction.

were evaluated according to their stabilization capacities in thermal shift assays where buffer acid-base pairs, ionic strength and additives were screened. The results exhibited a NaCitrate buffer pH 5-6 with NaCl concentrations above 700mM and additives like glycerol and Mn^{2+} as the optimal solution components (Fig.9.A). An immobilized metal affinity chromatography (IMAC) facilitated the elimination of most bacterial proteins while reasonably pure samples were retrieved after a gel filtration step (Fig.9.B and C). Even though the yield of purified proteins depended on the mutant, an average of 1mg of pure protein per liter of induced media was obtained reaching concentrations of 10mg/ml.

V. 1. 3. *In vitro* functional analysis of ANDV L_{200}

The nuclease activity of ANDV L protein N-terminal domain was determined according to the capacity of ANDV L_{200} mutants to degrade an isotope labeled 27mer ssRNA substrate. Given that a general two-metal ion mechanism is widely accepted to account for the phosphodiester bond hydrolysis. The absence of Mn^{2+}, documented as a stabilizer additive during the purification process (Fig.9.A), was used as the negative control of the pertinent enzymatic reactions. Along with all the mutants in the absence of Mn^{2+}, no substrate degradation was detected for mutants H36R, D97E, E110A and K124A even 2hupon addition of Mn^{2+}. The exchange of residues R35H, K44A, N50A, P96A and K127A allowed for vestigial ribonuclease activity. Whereas mutants D40E, I43A, N98A and N167A displayed considerable catalytic power, being N167A the most active with less than 3% of non-degraded substrate left after 1h incubation (Fig.10.A and B). The purity of all ANDV L_{200} mutants was confirmed to exclude the possibility of unknown proteins in the samples to be responsible for the observed outcomes in the reactions (Fig.10.C).

Nucleases of the PD…(E/D)…K superfamily can interact with different metal ions. To evaluate the binding ability of ANDV L_{200} mutants to Mn^{2+} or Mg^{2+}, the

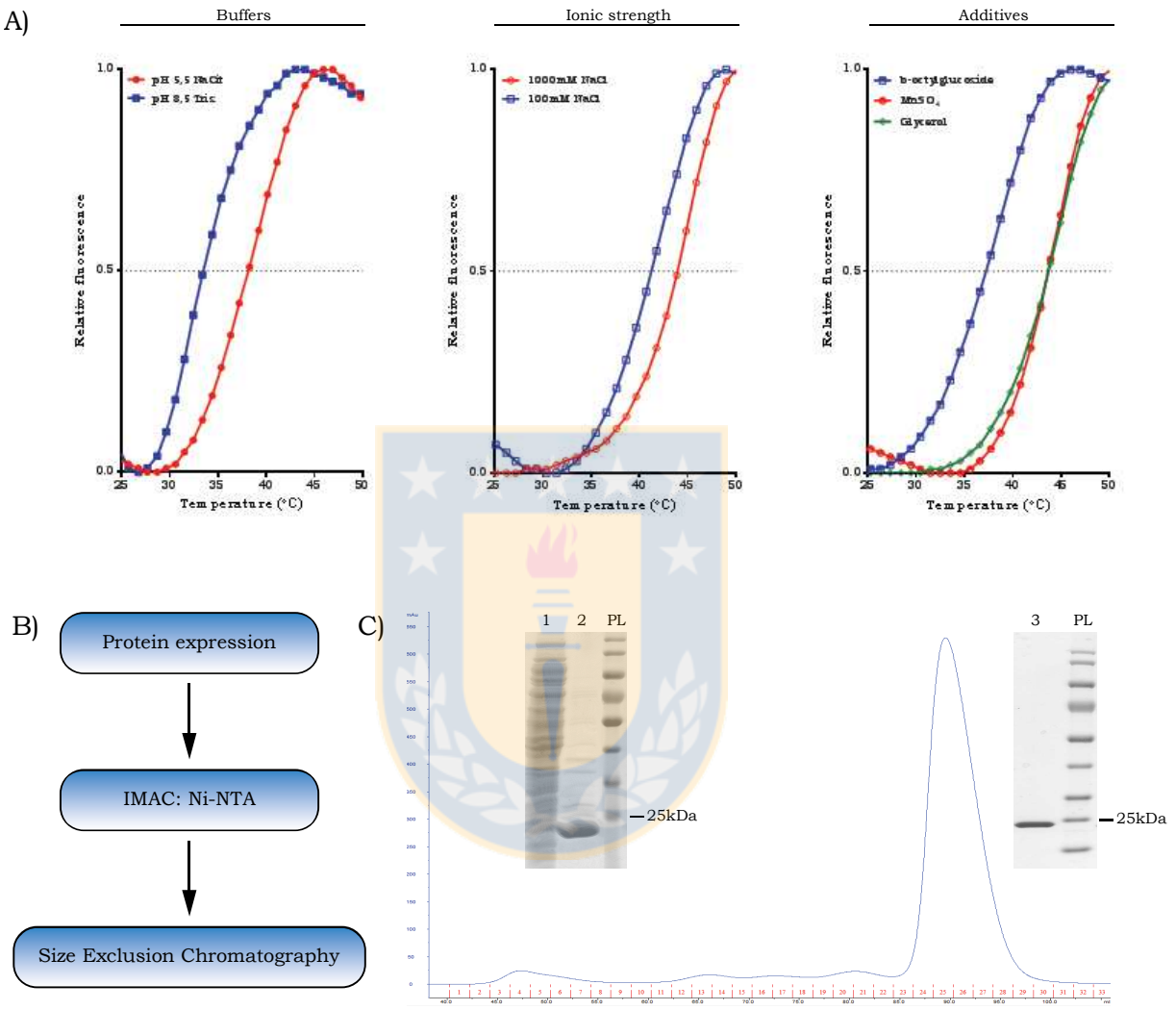

Fig.9. Purification process of ANDV L_{200} mutants. A) Selection of the optimal buffer solution components. The graphs show the relative fluorescence in relation to the melting temperature as measured by thermal shift assays for mutant K44A within different solution components. B) Workflow diagram of the purification process. C) Representative chromatogram for the size exclusion elution profile of samples used in biochemical studies. The internal images reveal the coomassie blue staining of 12% SDS-PAGE for the analysis of the purification steps. Lanes PL: protein ladder, 1: soluble fraction, 2: Ni-NTA elution, 3: size exclusion elution of ANDV L_{200} mutants.

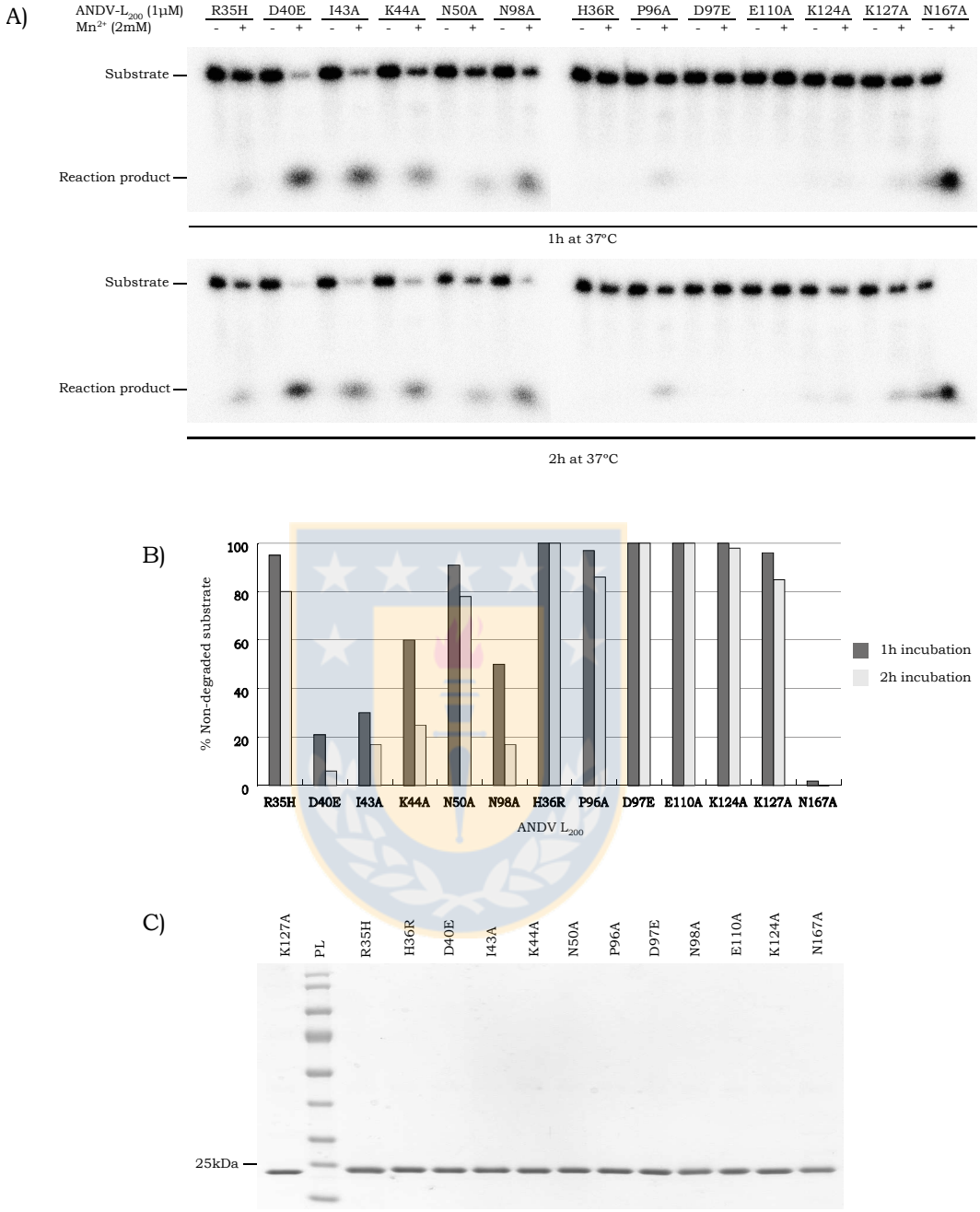

Fig.10. Catalytic activity of ANDV L protein N-terminal domain. A) Evaluation of the ribonuclease activity of ANDV L_{200} mutants via urea-polyacrylamide gel electrophoresis. Correspondingly, the upper and lower portion of the image shows the outcome of the same reaction mix after 1 and 2 h at 37°C. The assay components and expected radiolabeled species are detailed on top and to the left of the image respectively. B) Graphic representation of panel A, for the % of non-degraded substrate in relation to ANDV L_{200} mutants. C) Comassie blue staining of 12% SDS-PAGE for the analysis of ANDV L_{200} protein samples used in panel A. Lane PL: protein ladder.

most commonly used cofactors by nucleic acid modifying enzymes, thermal shift assays were performed in the absence and presence of both ions at 4 or 16 mM concentrations. Interestingly, the melting temperature (T_m) of mutants under 10mM EDTA, to ensure the chelation of metal ions carried over from the purification process, varied from 34.2 to 49.2 °C for the least and most stable ANDV L_{200} proteins I43A and K124A respectively (Fig.11.A and B). The majority of mutants, with the exception of D97E, suffered approximately a 7°C increase of their T_m in the presence of 4mM Mn^{2+} which continued to augment up to 15 °C in the presence of 16mM Mn^{2+}. In contrast, Mg^{2+} ions showed a much weaker effect (Fig.11.A and B). Since the higher T_m values implied the binding of divalent ions, presumably to the active site of ANDV L_{200} mutants, the unaltered stability of D97E suggested the participation of residue D97 in the coordination of the metal ions. Together with its inability to degrade the ssRNA oligo (Fig.10.A), D97E was used as a nuclease-dead mutant control in further enzymatic assays. The impact of these ions on the ribonuclease activity of ANDV $L_{200}$was analyzed using D40E, I43A, K44A, N98A, N167A and D97E. As mentioned before, none of the mutants degraded the substrate in the absence of divalent ions. Moreover, addition of Mn^{2+}, but not Mg^{2+}, rescued the activity of all expected mutants (Fig.11.C).

Because of the relaxed coordination geometry of Mn^{2+}, a binding of two such metal ions is often substrate independent and non-sequence specific (Yang 2011). To investigate if ANDV L_{200} had any substrate preference, mutants K44A, D97E and N167A, showing a range of enzymatic activities, were incubated with oligos of identical sequence but different nature (ss or ds RNA or DNA). The domain showed a ribose-backbone selective activity, with a less efficient cleavage of dsRNA as observed for the complete versus incomplete degradation of the corresponding ss and ds RNA by N167A (Fig.12.A). Surprisingly, an intermediate product was detected for the K44A and N167A catalyzed reactions when the ssRNA substrate was occupied. In addition, aspects as the length and secondary structures of ssRNA were analyzed by means of incubating

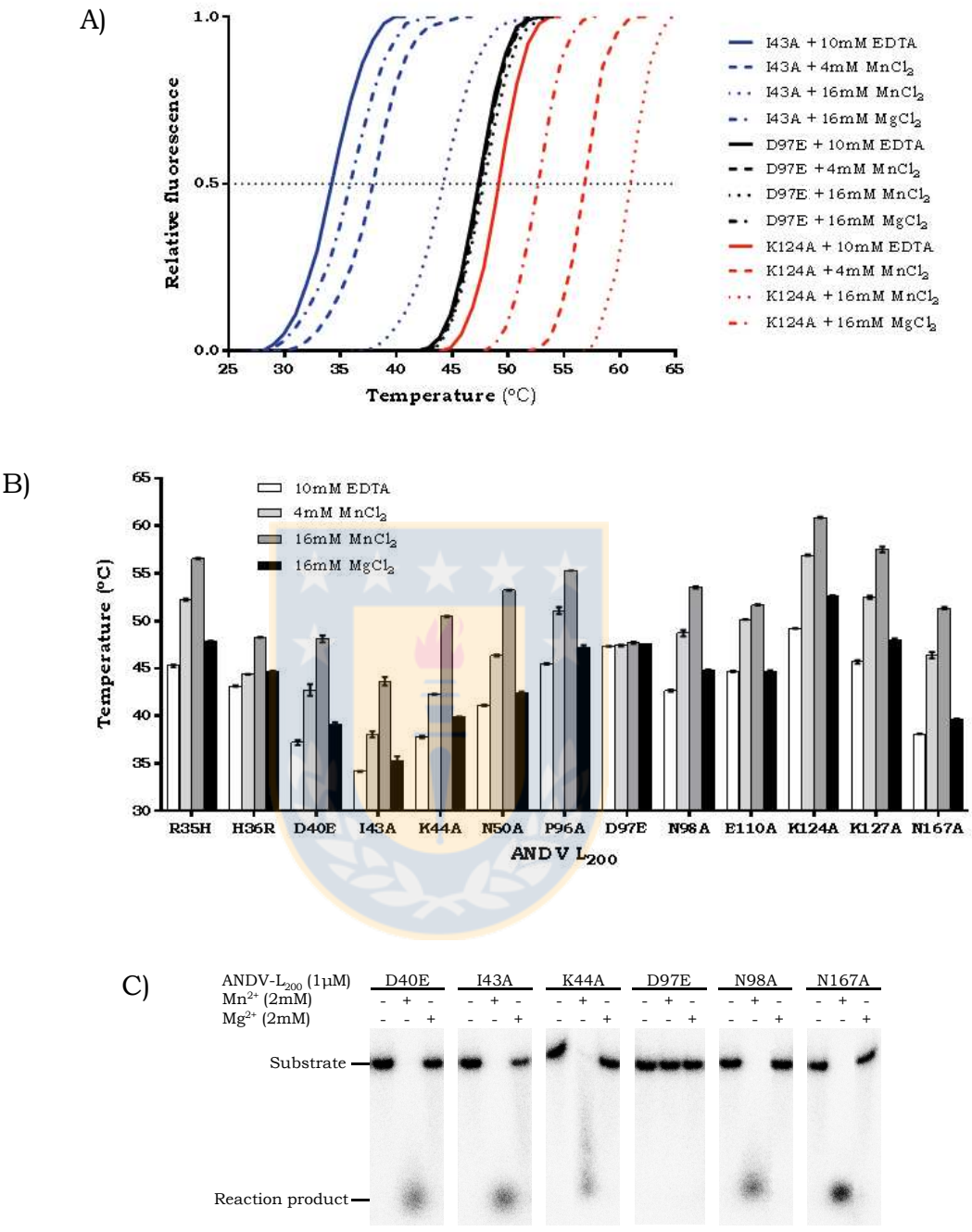

Fig.11. Divalent ion specificity of ANDV L_{200}. A) Representative alterations in the melting curves of mutants I43A, D97E and K124A as measured by thermal shift assays in the presence of 10mM EDTA, 4 and 16 mM of Mn^{2+} and 16mM of Mg^{2+}. B) Graphic depiction of the Tm values for all mutants analyzed as in A. The data represents the mean ± SD of four independent assays. C) Evaluation of the metal ion dependent ribonuclease activity of selected mutants via urea-polyacrylamide gel electrophoresis. The assay components and expected radiolabeled species are detailed on top and to the left of the image respectively.

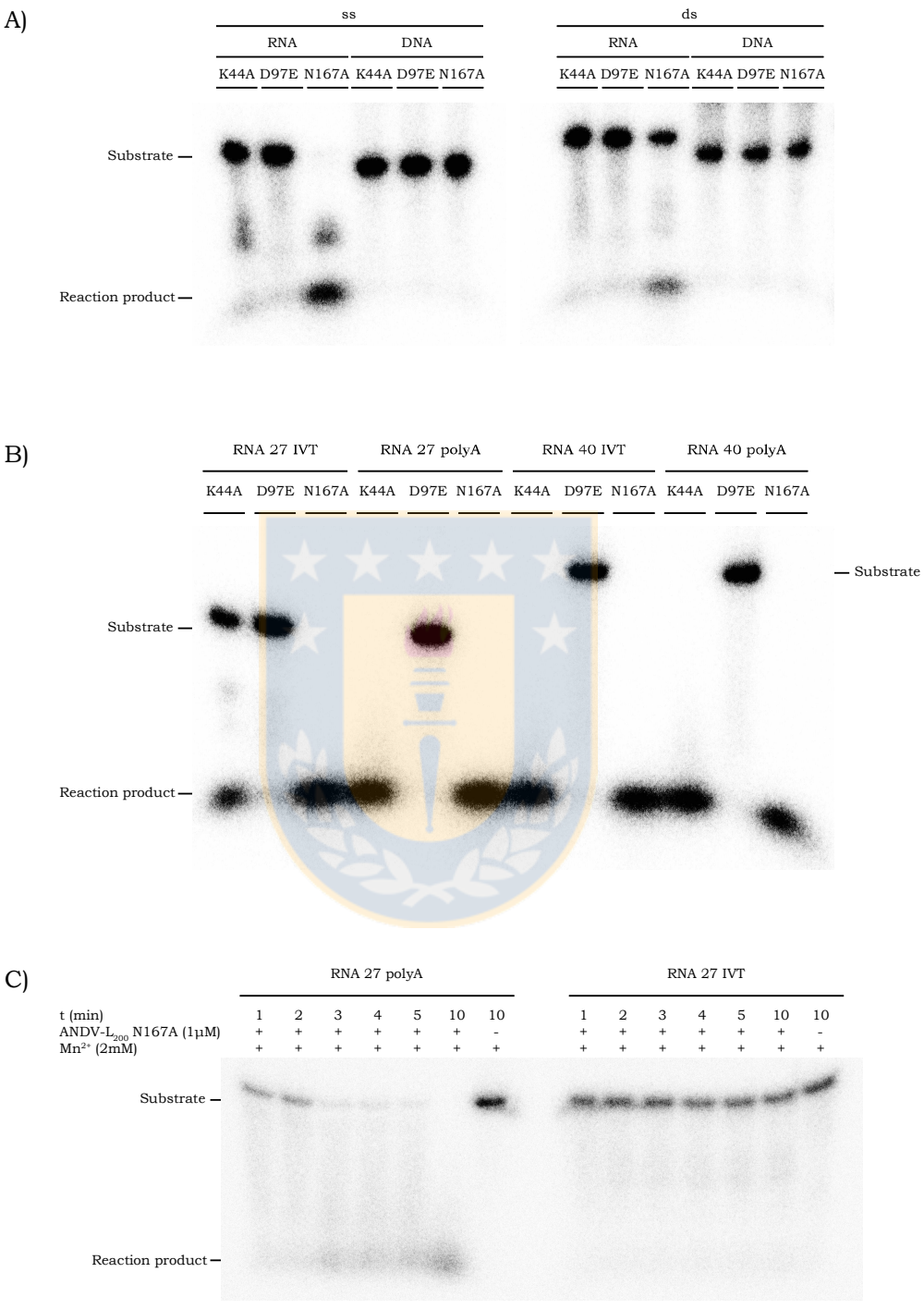

Fig. 12. ANDV L_{200} substrate preference. Evaluation of the effect of different A) nucleic acid types, B) lengths and C) secondary structures of substrates on the nuclease activity of selected mutants via urea-polyacrylamide gel electrophoresis. The assay components and expected radiolabeled species are detailed on top and to the sides of the image respectively.

these mutants with 27 or 40 mer structured (predicted Tm= 77 and 57 °C, respectively) or unstructured polyA primers. Longer and unstructured substrates seemed to be degraded faster being that K44A was only incapable to fully degrade RNA 27 IVT (Fig.12.B). Time courses of the unstructured and structured substrates cleavage by the strong activity of N167A confirmed the faster action of the domain over unstructured ssRNA where in 10min all this substrate was degraded compared to the minuscule amount of the structured RNA (Fig.12.C).

V. 2. Determine the structure of ANDV L protein endonuclease domain

V. 2. 1. Assessment of the crystallization sample

X-ray crystallography enables the detection of arranged atoms in three-dimensional space and takes advantage of the interatomic spacing of crystals by employing them as a diffraction gradient. A crucial step in this technique is to obtain well-diffracting crystals, in particular for macromolecular samples. Many factors influence the likelihood of crystallization of a protein. Although unpredictable, the quality of the starting material can dramatically increase the chances of success.

High purity and concentration are essential requirements met for all ANDV L_{200} mutants (Fig.9). However, the K127A domain alternative was chosen for structural studies as it was the most stable protein which retained the capacity to bind Mn^{2+} along with a residual nuclease activity (Fig.11.B and 10). Even though the structures of many tagged proteins have been resolved, it has been proven that the flexibility of those tags can diminish crystal nucleation, growth and diffraction quality. For this reason, a tag removal enzymatic reaction was included in the purification process (Fig.13.A and B). The end product homogeneity was determined via the gel filtration elution profile and corresponded to a monomeric state of the protein (Fig.13.B), which was thermostable according to the unchanged soluble yield following 72h

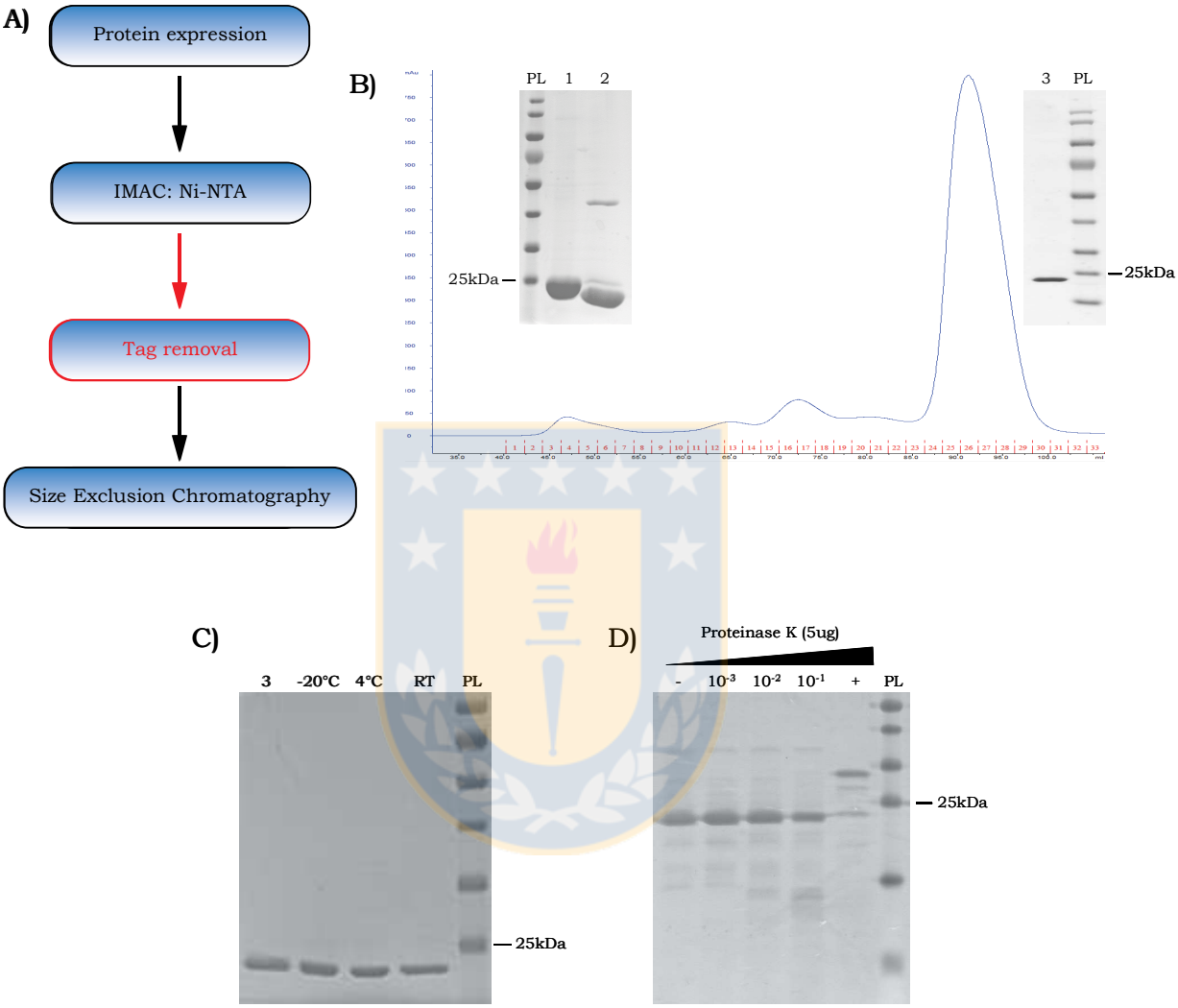

Fig.13. ANDV L_{200} K127A crystallization sample quality. A) Modified workflow diagram of the purification process. B) Representative chromatogram for the gel filtration elution profile of samples used in crystallization assays. The internal images reveal the coomassie blue staining of 12% SDS-PAGE for the analysis of the purification steps. C) Coomassie blue staining of 12% SDS-PAGE for the analysis of the domain thermostability. D) Coomassie blue staining of 16% SDS-PAGE for the analysis of conformational features by limited proteolysis. Lanes PL: protein ladder, 1: Ni-NTA elution, 2: HRV-3C digestion product, 3: gel filtration elution of ANDV L_{200} K127A, -20°C: flash frozen protein stored at -20°C, 4°C: protein stored at 4°C, RT: protein stored at room temperature.

incubation at different temperatures (Fig.13.C). Furthermore, a high level of compaction was detected for the protein domain by limited proteolysis (Fig.13.D).

V. 2. 2. Solve the atomic structure of ANDV L_{200}

The primary screen for crystallization conditions revealed different settings that yielded protein crystals, these contained pH 5-7 in buffers and either PEG 3350 or Jeffamine M-600 as precipitants (Fig.14.A). The optimization of hit conditions produced thin plate crystals within 24h of mixing 10mg/ml ANDV L_{200} K127A with 100mM NaAc pH 5, 2mM $MnCl_2$, 27.5% PEG 3350 and 500mM $(NH_4)_2SO_4$ at 22°C (Fig.14.B). These crystals diffracted to 2.4Åand contained one molecule per asymmetric unit in space group $P42_12$ (Table.1).

ANDV L_{200} K127A structure was solved by molecular replacement using the endonuclease domain of HNTV (kindly provided by Dr. Juan Reguera, PDB ID: submitted) as a search model. Clear electron density was visible for the complete structure with the exception of the loop between α_1 and α_2–helices where the signal was weak, allowing for the building of a contiguous polypeptide chain (Fig.14.C and 15.A). Diffraction data collected at 1.77Å permitted the calculation of an anomalous difference electron density map that verified the presence of a Mn^{2+} ion bound to the active site (Fig.15.A and B).

The overall structure of the domain has a central portion formed by β-sheets (β_1, β_2 and β_3) which divides the remaining helical elements in two diagonal lobes (Fig.15.A). As viewed in figure 15.A, the top lobe contains α-helices (α_1, α_2, α_7 and α_8) from the N and C –terminal ends of the protein with interactions between residues in the last turn of the α_8-helix and the first turn of the α_2-helix stabilizing this helix bundle. Meanwhile the bottom lobe contains α-helices (α_3, α_4, α_5 and α_6) and much more flexible regions represented as long loops. Most of the surface area is formed by the helix bundles and among the lobes lays a groove culminating in the negatively charged active site pocket

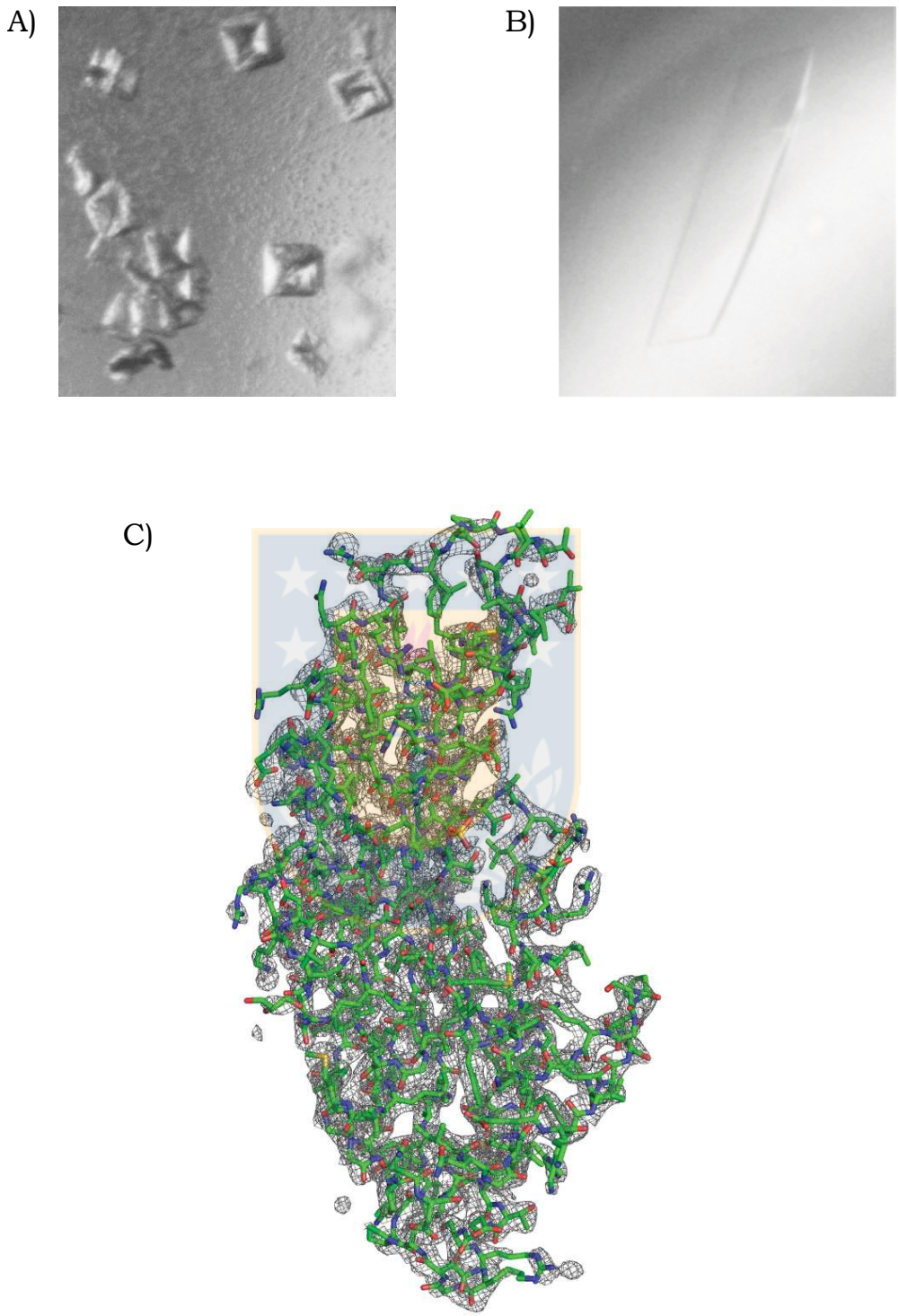

Fig.14. ANDV L_{200} K127A crystals. Photograph of representative crystals at 40X from A) screened and B) optimized conditions. C) Electron density map 2m*F*o-D*F*c at 1σ (gray mesh) obtained from an optimized crystal occupied by stick representation of ANDV L_{200}K127A.

ANDV L_{200}-K127A	Native	Anomalous
PDB ID: 5HSB		
Data collection		
Space group	P 4 2_1 2	P 4 2_1 2
Cell parameters		
a, b, c (Å)	82.89, 82.89, 79.31	82.89, 82.89, 79.31
α, β, γ (°)	90, 90, 90	90, 90, 90
Wavelength (Å)	0.984	1.77
Resolution range (Å)	79.31-2.36 (2.44-2.36)	79.31-2.8 (3.1-2.8)
# total/unique reflections	84120/20577 (18266/4391)	93605/13170 (18108/2446)
Completeness (%)	99	100
Redundancy	4.1 (4.2)	7.1 (7.4)
Average I/σ(I)	19.3 (2.1)	14.2 (1.8)
R_{merge} (%)	4.9 (98)	10.9 (126.9)
Refinement		
Resolution (Å)	79.31-2.36 (2.44-2.36)	
# relections	11856 (1164)	
R_{work}/R_{free} (%)	22.02/27.44 (35.16/48.42)	
# atoms	1692	
Protein	1612	
Ligands	22	
Solvent	201	
Average B-factor (Å^2)	72,77	
Protein	72,4	
Ligands	90,1	
Solvent	76,43	
RMSD		
bond distance (Å)	0,008	
bond angle (°)	1,09	
Ramachandran plot		
Favored regions (%)	96	
Allowed regions (%)	4	
Outlier regions (%)	0	

Highest resolution shell values are shown in parentheses.

Table.1. Crystallographic data collection and structure refinement statistics.

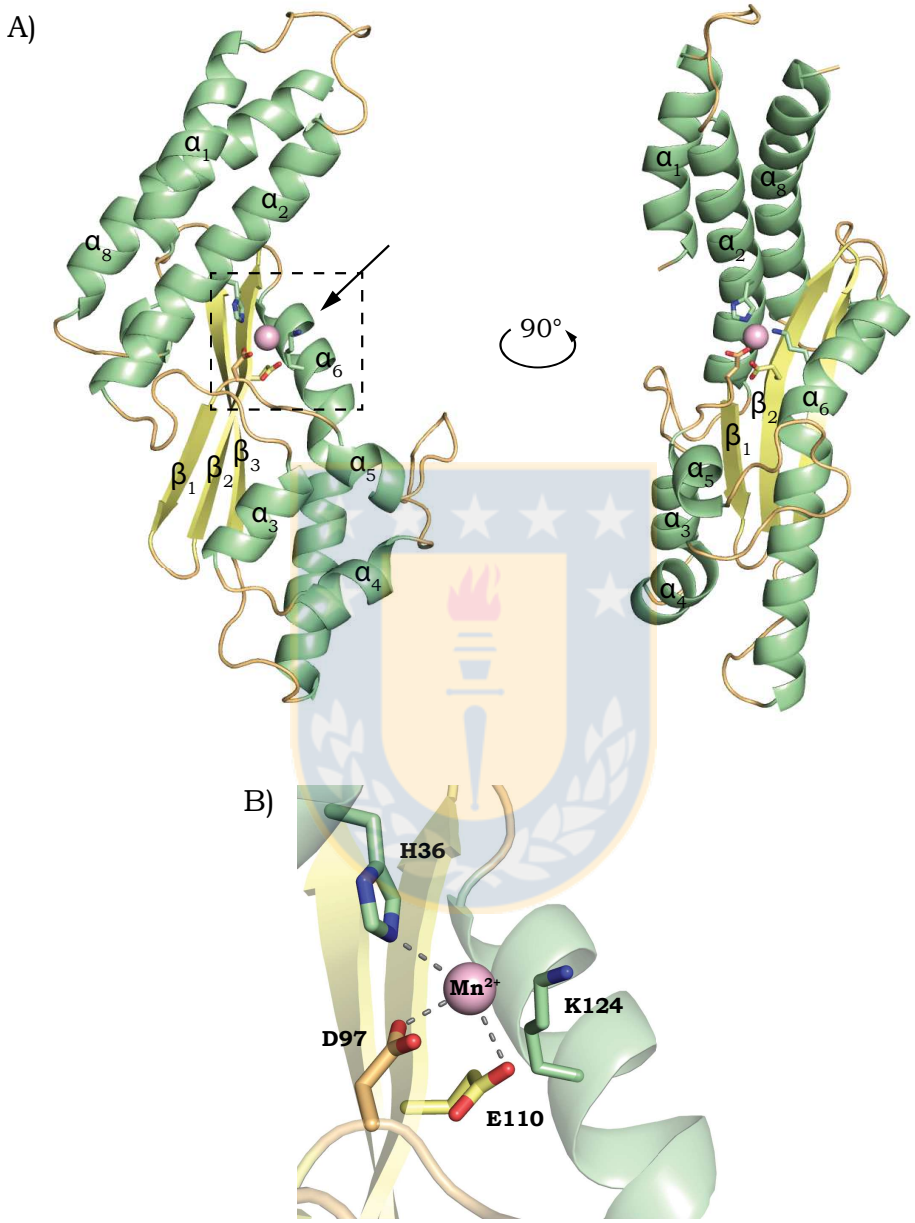

Fig.15. ANDV L_{200} K127A structure. A) Ribbon diagram of the overall structure (PDB ID: 5HSB). Secondary structures α-helices (green), β-sheets (yellow) and loops (orange) are annotated with consecutive numbers. The purple sphere represents a Mn^{2+} ion within the framed active site indicated with an arrow. B) Zoom of the active site framed in A. Side chain of the Mn^{2+} coordinating residues established by dashed gray lines and the putative catalytic lysine are shown as sticks.

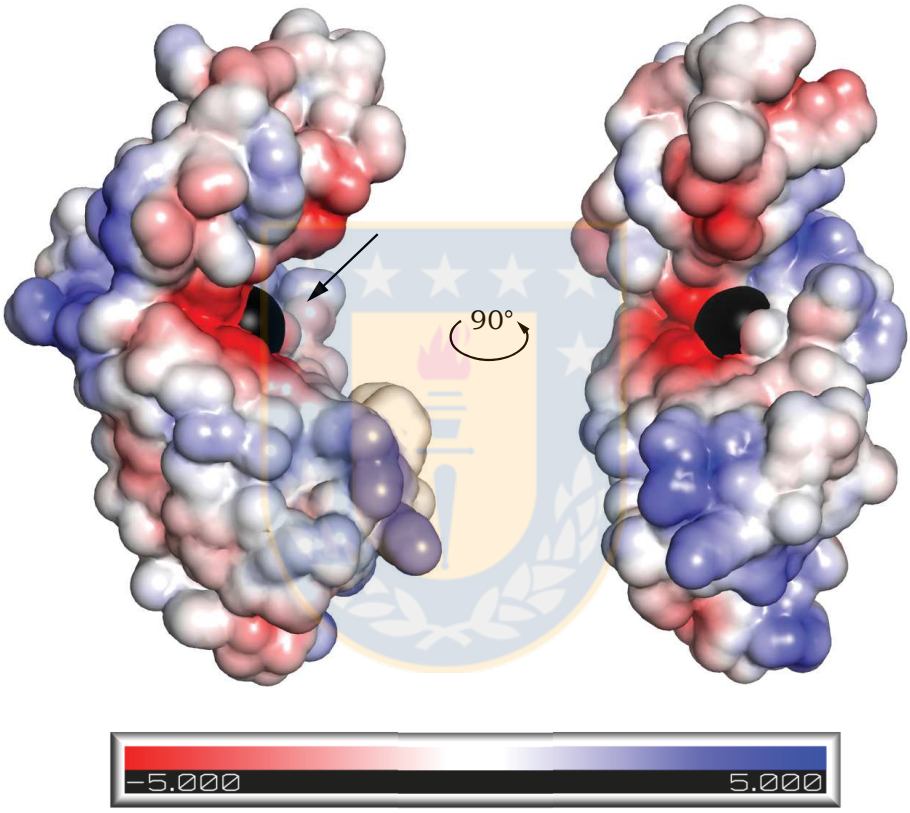

Fig. 16. Surface charge distribution of ANDV L_{200} K127A. The electrostatic surface potential is shown from -5KT/e in red to +5KT/e in blue. The black sphere marks the active site indicated with an arrow.

(Fig.16). Active site residues H36, D97 and E110 coordinate the Mn^{2+} ion found in the structure while K124 is found 3.7 Å from the metal ion (Fig.15.B), a reasonable distance for it to be considered the putative catalytic lysine in the two-metal ion mechanism proposed for sNSVs endonucleases.

V. 2. 3. Comparison with other sNSVs L protein endonuclease domain

The PA protein from IFV is by far the most studied cap-snatching endonuclease of sNSVs. Considering the lack in sequence homology between ANDV L_{200} and IFV PA proteins, except for the conserved PD…(E/D)…K nuclease motif, the overall structure is surprisingly similar (Fig.17.A and B). The core of both molecules is formed by central β-sheets, different in number, which divide the remaining helical elements, different in length and distribution, in two diagonal lobes. These lobes create a groove between them where the active site is located. Together with the central β-sheets, α-helices α_2 and ANDV α_6 or IFV α_5 provide the same arrangement of the crucial active site residues (Fig.17.C). In contrast to the single Mn^{2+} ion found in ANDV L_{200}, two ions of the same metal were detected in the active site of IFV PA (PDB ID: 2W69). Another obvious difference between these endonucleases is the shape of the domains. Compared to the compacted IFV PA protein, ANDV $L_{200}$is elongated and flat with approximately outer dimensions of 67 × 35 × 30 Å (Fig.17.A and B).

V. 3. Evaluate the potential of ANDV L protein endonuclease domain as a pharmacological target

V. 3. 1. Determine the effect of DPBA on ANDV L_{200} mutants

The vital mRNA capping mechanism of sNSVs involves viral exclusive molecules like the cap-snatching endonuclease. As shown above, the active site structure of this enzyme is highly conserved thus it can serve as an attractive target for drug discovery against a broad spectrum of pathogenic viruses.

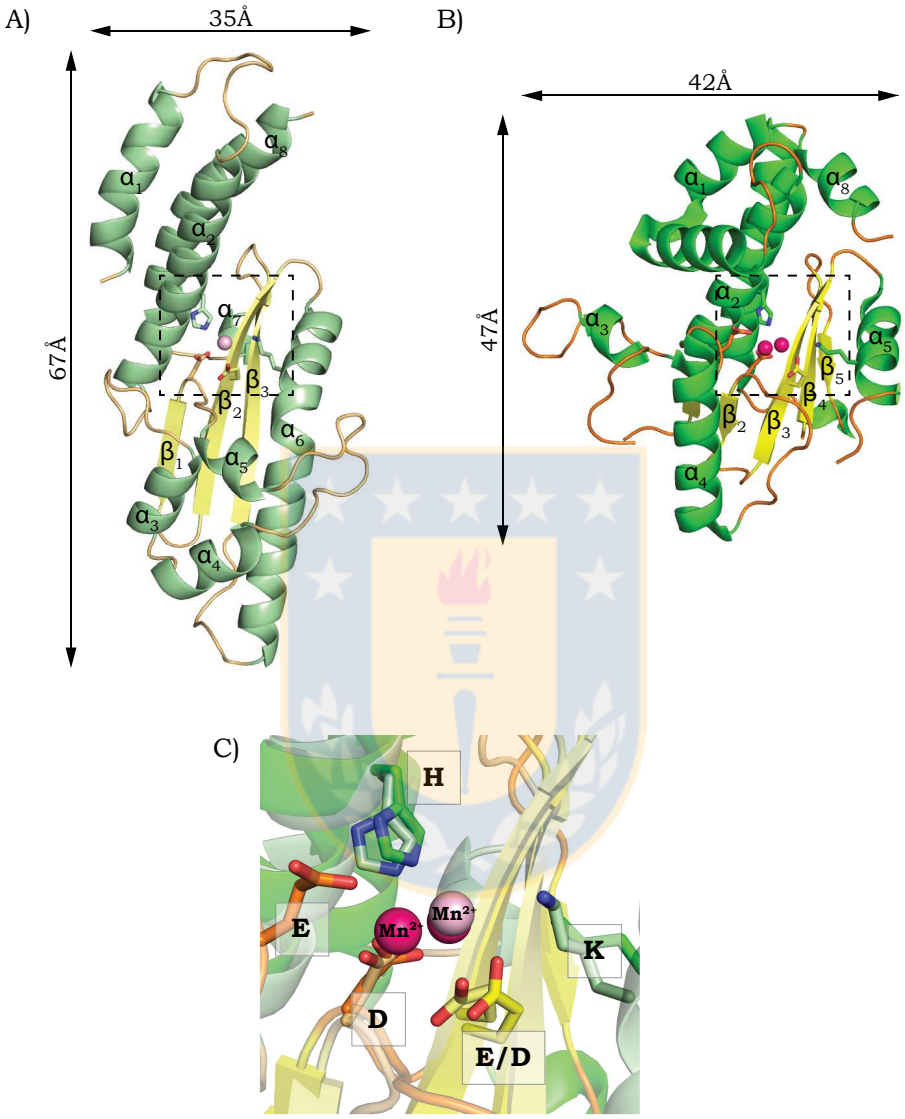

Fig.17. Evolutionary conservation of sNSVs endonuclease domain structure. Ribbon diagram of the overall structures of A) ANDV L_{200} K127A (PDB ID: 5HSB) and B) IFV PA (PDB ID: 2W69). Secondary structures α-helices (green), β-sheets (yellow) and loops (orange) are annotated with consecutive numbers. The purple and pink spheres represent the Mn^{2+} ions within the framed active. C) Zoom of the superimposition of the active sites framed in A and B. Side chain of the Mn^{2+} coordinating residues and the putative catalytic lysines are shown as sticks.

ANDV L_{200} suitability for future antiviral high-throughput screening was assessed through biochemical assays using the classical IFV PA inhibitor DPBA. A preliminary appraisal of DPBA interaction within the active site of the domain was obtained as consequence of the improved stability of mutants K44A and N167A compared to D97E, residue implicated in the Mn^{2+} ion coordination, upon addition of the compound according to the T_m values measured by thermal shift assays in the presence of 10mM EDTA, 4mM $MnCl_2$ or 4mM $MnCl_2$ plus 25µM DPBA (Fig.18.A).The significance of this binding to ANDV L_{200} ribonuclease activity was determined incubating mutant N167A with ^{32}P-labeled substrate under increasing amounts of DPBA. Evaluation of the reactions outcome disclosed a dose-dependent inhibition of the enzymatic activity within the µM range (Fig.18.B and C).

V. 3. 2. Analyze the *in vitro* antiviral activity of DPBA on ANDV growth

To elucidate if ANDV endonuclease inhibitors can be used to impair the virus multiplication, the antiviral activity of DPBA was assessed via an infectious cell culture experiment. Hantaviruses are known to have slow growth rates, which translates into low titers, when propagated in cell cultures. If not taken into consideration, such features can lead to the incorrect interpretation of the effect of compounds on the virus amplification. For this reason, growth curves for the available ANDV strain were generated using different types of cell lines. In correspondence with previous reports HEK-293 cells were not susceptible to ANDV infection (Mackow & Gavrilovskaya 2001), whileVeroE6 and BHK-21 cells produced similar amounts of viral titers. Nevertheless, ANDV grew faster in VeroE6 cells reaching 10^4 FFU/ml in 3 days (Fig.19.A).With this in mind, VeroE6 cells were selected to test the impact of DPBA on ANDV titers at 3 days post-infection. An effective *in vitro* and *in vivo* antiviral with an unrelated mechanism of action like RBV was used in parallel as control for the methodology (Safronetz et al. 2011). Unfortunately, treatment of ANDV infected VeroE6 cells with DPBA did not show a reduction of the infectious viral

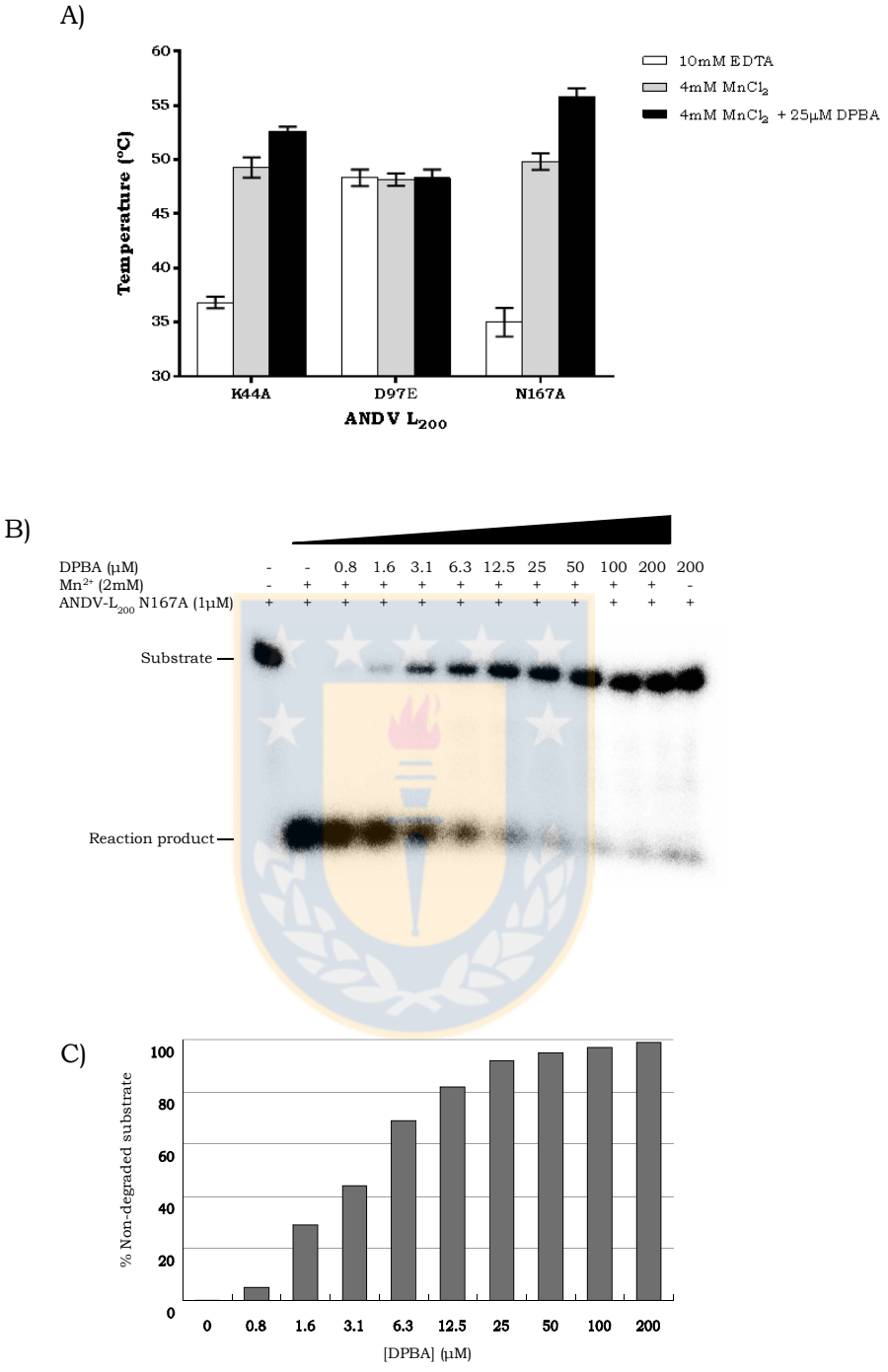

Fig.18. Biochemical analysis of DPBA effect on ANDV L_{200}. A) Stability of selected mutants in the presence of EDTA, $MnCl_2$ or $MnCl_2$ + DPBA. The graph shows the mean Tm values ± SD of four independent assays. B) Evaluation of the ribonuclease activity of mutant N167A under increasing amounts of DPBA via urea-polyacrylamide gel electrophoresis. The assay components and expected radiolabeled species are detailed on top and to the left of the image respectively. C) Graphic representation of panel B, for the % of non-degraded substrate in relation to increasing concentrations of DPBA.

A)

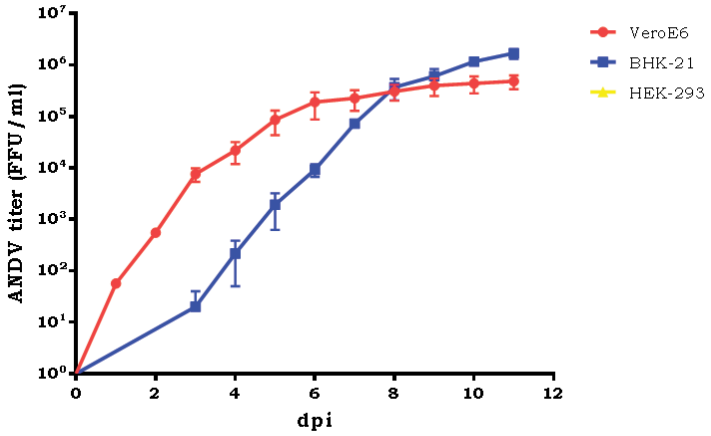

B)

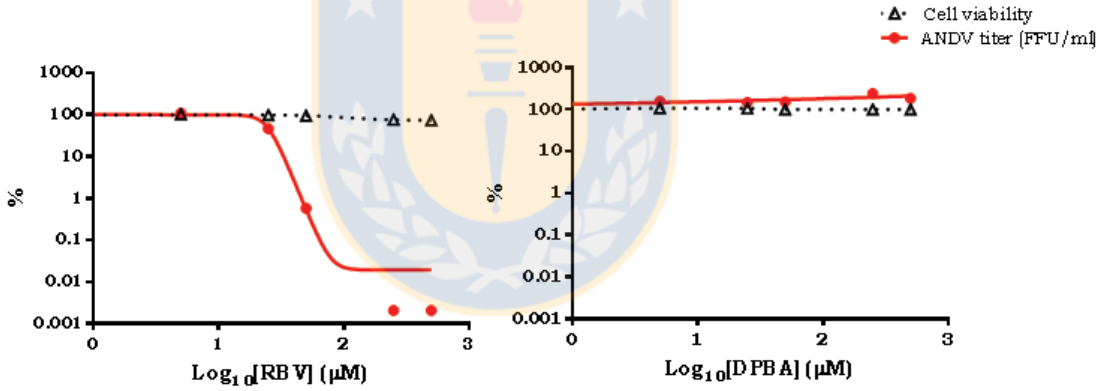

	RBV	DPBA
IC_{50}	24.26 µM	-
IC_{90}	32.81 µM	-
IC_{99}	45.61 µM	-

Fig.19. Antiviral activity of DPBA against ANDV in cell culture. A) Permissiveness of cell cultures to ANDV. B) Dose-response curves for RBV and DPBA fitted to the data points representing mean ANDV titers ± SD of an experiment performed in triplicates. The IC_{50}, IC_{90} and IC_{99} values were calculated from the respective sigmoidal functions with 95% confidence interval (95% CI). Cell viability under compound treatment was determined by MTT method.

particles generated (Fig.19.B). As expected for RBV a dose-dependent 3 logs drop of the virus yield was observed with a half maximal inhibitory concentration (IC_{50}) of approximately 24μM. It is worth mentioning that unlike DPBA, RBV concentrations above 250μM displayed cell viabilities lower than 80% as estimated via MTT tests (Fig.19.B).

VI. DISCUSSION

VI. 1. Characterize the *in vitro* nuclease activity of ANDV L protein N-terminal domain

Research concerning ANDV L protein has been challenging, in particular due to the inability to be detected either during infection or heterologous expression in mammalian cells (Brown et al. 2012; Heinemann et al. 2013; Chiang et al. 2014). The present work goes further and exposes the deleterious effect of the molecule N terminus on BL21-Gold(DE3) bacteria since only cells transformed with the wt insoluble constructs, thus inactive, were recovered (Fig.6). The death of *E. coli* strains which harbor the λ (DE3) prophage can be explained by the leaky expression of highly toxic genes placed downstream T7 promoters (Saïda et al. 2006). Such a level of toxicity is unprecedented for the cap-snatching endonuclease of sNSVs. The use of single amino acid mutant alternatives (R35H, H36R, D40E, I43A, K44A, N50A, P96A, D97E, N98A, E110A, K124A, K127A and N167A) enabled bacterial growth under the production of soluble proteins, which implied their later confirmed attenuated nuclease activities (Fig.8 and Fig.10). The fact that Y32V and D37A mutant constructs mimicked the wt lethal behavior in bacteria, in contrast to their full-length expression in mammalian cells, let speculate about the regulatory influence of the rest of the L protein over the amino terminal catalytic power. Coherent with the allosteric modulation of the polymerase activity of LACV L protein by its distinct site interaction with both ends of the vRNA which induces conformational rearrangements in the catalytic site (Gerlach et al. 2015). It becomes logical to assume that hantaviruses must have a system in infected cells to control the putative endonuclease activity of the L protein.

ANDV L N-terminal domain was identified as the first 200 residues of the protein being that they were a requirement for solubility and biological function

(Fig.7 and Fig.10). Through the analysis of the atomic structure of ANDV L_{200} K127A it can be assumed that interactions between residues in the last turn of the α_8-helix and the first turn of the α_2-helix are responsible for the domains stability (Fig.15.A). Accordingly, protein constructs excluding residues L198 and I199 were misfolded and found in inclusion bodies (Fig.7).

The residue exchanges in the domain influenced the expressed levels of proteins (Fig.8.B). Curiously, yields did not correlate with the generation times of the transformed bacteria but with the molecules stability and enzymatic activity (Fig.8.A, Fig.11.B and Fig.10). It can be argued that protein induction begins at an equally desired OD and this imposes a metabolic burden that drastically decreases bacterial growth rate thus differences provided in the number of cells is negligible. However, comparing the generation times of 32min for the nuclease-dead mutant D97E with 41min for the most active mutant N167A there is a clear connection between bacteria viability and the domains catalysis (Fig.8.A and 10).

For any enzymatic assay it is primordial to have pure protein. Exposure of the added N-terminal His-tag, selection of optimal buffer components and size exclusion chromatography facilitated the obtainment of samples clean from contaminants which could interfere with biochemical assays (Fig.9 and Fig.10). Therefore, non refutable proof was provided for the existence of a Mn^{2+} dependent endoribonuclease domain in the N terminus of ANDV L protein. In analogy to previously described sNSVs cap-snatching endonucleases, ANDV exhibited a divalent ion dependency for the hydrolysis of phosphodiester bonds (Fig.10 and Fig.11) (Dias et al. 2009; Morin et al. 2010; Reguera et al. 2010; Wallat et al. 2014). Consistent with this, mutation of residues directly involved in the metal ions coordination H36, D97 and E110 abolished catalytic activity despite presence of Mn^{2+} (Fig.10 and Fig.15.B). Moreover, the documented specificity for Mn^{2+} over Mg^{2+} can be indicative of non-sequence specific cleavage while been selective for ribose-backbone substrates (Fig.11 and Fig.12)

(Yang 2011). At least for the isolated domain there was no need of a cap structure for substrate recognition or enzymatic activity. This alludes to the proposed existence of a cap-binding domain at the C-terminal region of the L protein (Gerlach et al. 2015). Attention is drawn to the exclusive degradation of RNA since IFV and LACV endonucleases have also processed ssDNA *in vitro* (Dias et al. 2009; Reguera et al. 2010). Although both ss and ds RNA are degraded by ANDV L_{200}, presumably the higher accessibility of unstructured ssRNA compared to structured dsRNA justifies a faster catalysis (Fig.12.A and C). It is worth mentioning that ss oligos used to generate ds substrates might linger in the sample after the hybridization process. Thus we can´t exclude the possibility that reaction products detected in the analysis of dsRNA cleavage are the result of ss substrate degradation. On the other hand, it is plausible to suspect that longer substrates, 40mer versus 27mer, have higher binding affinities which result in lower percentages of non-degraded substrate (Fig.12.B). Hantaviruses lack a robust replicon system capable of deciphering the direct contribution of the N-terminal domain of the L protein to the cap-snatching mechanism (Brown et al. 2012). However, the accumulation of intermediate products observed for incomplete reactions suggests the endonuclease activity expected from the described phenomenon (Fig.12.A) (Garcin et al. 1995).

VI. 2. Determine the structure of ANDV L protein endonuclease domain

The atomic structure of ANDV L_{200} K127A is the first published hantaviral cap-snatching endonuclease. Like many others, this study reveals the high conservation of protein folds throughout evolution (Ingles-Prieto et al. 2013). Although nearly absent sequence identities are found between sNSVs endonucleases, IFV (PDB ID: 2W69) and ANDV (PDB ID: 5HSB) structures denote common features (Fig.17). Both consist of 2 lobes with the conserved active site buried in a cavity accessed via a groove flanked by the lobes. Interestingly, positively charged patches surrounding ANDV L_{200} active site may

contribute to the affinity of the enzyme for the negatively charged RNA substrates (Fig.16). Whether or not this feature plays a role in the toxic endonuclease activity upon recombinant expression remains to be determined.

A closer look at their active sites highlights the almost perfect superimposition of the side chains of residues essential for catalysis (Fig.17.B). However, in opposition to the 2 Mn^{2+} ions observed for IFV, the crystal structure for ANDV exhibits a single Mn^{2+} ion in the active site. Such discrepancy may be explained by a low affinity for the second Mn^{2+} ion as seen for related endonucleases (personal communication with Dr. Juan Reguera). The collected thermal shift data supports this idea since the stability of the domain increases together with concentrations of Mn^{2+} for roughly 10 times the 2mM present at the crystallization conditions (Fig.11.A and B). By virtue of the domain conservation and its common metal ion, it is safe to assume that the second Mn^{2+} in the structure of ANDV could occupy a position analogous to its counterpart in IFV. In accordance to the structure, it also makes sense that the mutation of D97, which would coordinate both Mn^{2+} ions, had the strongest effect on metal binding. Hence it is reasonable to propose a universal two-metal ion dependent nucleolytic mechanism for cap-snatching endonucleases.

By combining the biochemical properties of ANDV L_{200} mutant proteins with the location in the structure of the mutated residues, it is feasible to group them according to the inferred roles (Table.2). Active site residues essential for endoribonuclease activity gather H36, D97, E110 and K124. Residues involved in the stabilization of the active site cavity clusters D37 and P96 which position central Mn^{2+} ion coordinating H36 and D97, respectively. Also D40, K44, N50 and N98 that form hydrogen bonds with each other and main chain atoms to fix loop 5 containing D97. Additionally, I43 contributes to the hydrophobic steadiness of the β-sheets core of the domain while K127 possibly places the incoming substrate into the active site cavity. The arrangement of Y32 and R35 at the entrance of the groove lets to speculate that these are residues involved

ANDV-L_{200}	Expression level in mammalian cells*	Expression level in bacteria cells	Comparative stability	Mn^{2+} binding	Nuclease activity	Location in structure
wt	-	x				
Active site residues essential for activity						
H36R	+++	+++	++	-	-	helix α2
D97E	+++	+++	+++	-	-	loop 5
E110A	+++	+++	+++	+	-	strand β2
K124A	+++	+++	+++	+	-	helix α6
Residues involved in the stabillization of the active site cavity						
D37A	+	x				
D40E	+++	+	+	+	+++	helix α2
I43A	+++	+	+	+	++	helix α2
K44A	+++	+	+	+	+	helix α2
N50A	+	+++	++	+	+	loop 2
P96A	+++	++	+++	+	+	loop 5
N98A	+	+	++	+	++	strand β1
K127A	++	++	+++	+	+	helix α6
Residues involved in substrate binding						
Y32V	++	x				
R35H	+++	+++	+++	+	+	helix α2
Residue involved in the overall structure stabilization						
N167A	+	+	+	+	+++	loop 9

Table.2. Summary of ANDV L_{200} mutants properties and the hypothetical role of mutated residues. The discrimination criterion is explained below.
Expression level in mammalian cells, (*) in the context of the full-length protein, estimated from western-blot signals shown by Heinemann et al. 2013; "-" undetected, "+" low, "++" medium and "+++" high signal intensities respectively.
Expression level in bacteria cells estimated from protein yield; "x" deleterious to cells, "+" ≤ 0.5mg/L, "++" 0.5-1 mg/L and "+++" ≥ 1mg/L.
Comparative stability as the respective T_m measured by thermal shift assays; "+" ≤ 40°C, "++" 45-40 °C and "+++" ≥ 45°C.
Mn^{2+} binding as the respective increase in the T_m measured by thermal shift assays; "-" ≤ 2.9°C and "+" ≥ 3°C.
Nuclease activity as the percentage of non-degraded substrate at 1h incubation; "-" 100%, "+" 50-100 %, "++" 25-50 % and "+++" ≤ 25%.

in substrate binding. Many studies have documented a preference of amino acids at RNA binding sites, within which are the positively charged arginine and the aromatic tyrosine (Jones et al. 2001; Baker & Grant 2007). Distant from the active site, N167 stabilizes the overall structure via hydrogen bonds with the β_3-sheet. In agreement with the peripheral location of N167, the corresponding mutant shows the slowest growth of transformed bacteria and is the least attenuated.

VI. 3. Evaluate the potential of ANDV L protein endonuclease domain as a pharmacological target

It is of public health interest to develop treatment options for patients with hantavirus infections. Considering that vascular leakage is the main underlying complication and that it appears to be associated with infected endothelial cells, countermeasures aimed at preventing virus replication might be effective even after the onset of symptoms (Wahl-Jensen et al. 2007). Moreover, antiviral candidates against conserved viral proteins domains and their vital associated activities, like the ANDV cap-snatching endonuclease characterized in this work, possibly will have broad spectrum usages.

The IFV PA endonuclease has been used as a target in drug discovery programs and several specific inhibitors have been found (Baughman et al. 2012; DuBois et al. 2012). Including these is DPBA, which has shown to reduce the domain enzymatic activity *in vitro*. The structure of the co-crystallized IFV PA protein-compound complex revealed that DPBA interacts directly with the 2 active site metal ions. Likewise, thermal shift assays employing ANDV L_{200} mutants of residues not implicated in divalent ion coordination K44A and N167A, as opposed to D97E, confirmed an enhanced stability upon addition of DPBA (Fig.18.A). Whilst the *in vitro* nuclease experiments provided proof of concept that the ribonuclease activity of the domain is amenable to compound screening, mutant N167A emerged as the most promising candidate for this

purpose (Fig.18.B and C). Unfortunately, the attempt to validate the effect of DPBA on ANDV growth failed. Perhaps concentrations higher than 500μM are needed or in a more probable scenario the compound did not enter the cells. The provided structural insight of ANDV endonuclease will certainly facilitate the optimization of small molecules like DPBA, either by improving its affinity or metabolic half life, targeting the L protein. Consequently such compounds could restrict the virus replication ergo its dissemination, thus acting as promising antivirals.

VII. CONCLUSIONS

Up to now, the heterologous expression of the isolated N-terminal domain of ANDV L protein has not been published. The present study has reported the deleterious effect of its wild-type enzymatic activity in bacteria and has documented single amino acid mutations that can circumvent such toxicity. This domain contained the first 200 residues of the protein which harbored a Mn^{2+} dependent endoribonuclease. The methodology described for the production of catalytic active mutants may indirectly contribute to the future discovery of potential antivirals. Moreover, the novel crystal structure allows for the optimization of hit compounds to improve features as binding affinities and metabolic half life. As it is shown that the active site of sNSVs cap-snatching endonucleases is highly conserved and essential in virus amplification, it seems possible to design broad spectrum drugs against a wide range of pathogenic viruses.

The continuity of this work will focus on the development of an adequate high throughput screening assay that enables the *in vitro* identification of small molecules capable of hampering ANDV growth in cell cultures. Finally, the discussed structure-function relationship of mutated residues will also help in the selection of attenuated full length L proteins to be used in ANDV RNA synthesis research.

VIII. ABREVIATIONS

Ab: antibody

ANDV: *Andes virus*

APS: ammonium persulfate

ATP: adenosine triphosphate

BSL: biosafety level

cDNA: complementary RNA

CO_2: carbon dioxide

cRNA: complementary RNA

DEPC: diethylpyrocarbonate

DMEM: Dulbecco´s modified eagle´s medium

DNA: deoxyribonucleic acid

DPBA: 2,4-dioxo-4-phenylbutanoic acid

dpi: days post-infection

ds: double-stranded

DTT: dithiothreitol

EDTA: ethylenediaminetetra acetic acid

ELISA: enzyme-linked immunosorbent assay

ER: endoplasmic reticulum

FBS: fetal bovine serum

GTP: guanosine triphosphate

HCPS: hantavirus cardiopulmonary syndrome

HNTV: *Hantaan virus*

HRP: horseradish peroxidase

HRV-3C: human rhinovirus 3C

IFA: indirect fluorescent antibody test

IFV: *Influenza virus*

IgG: immunoglobulin G

IgM: immunoglobulin M

IL28B: interleukin 28B

IMAC: immobilized metal affinity chromatography

IPTG: isopropyl β-D-1-thiogalactopyranoside

LACV: *La Crosse virus*

LASV: *Lassa virus*

LB: lysogeny broth

LCMV: *Lymphocytic Choriomeningitis virus*

MEM: minimal essential medium

MOI: multiplicity of infection

mRNA: messenger ribonucleic acid

NCR: noncoding regions

NP: nucleoprotein

NSs: non-structural protein

NTP: nucleoside triphosphate

OD: optical density

ORF: open reading frame

pAb: polyclonal antibody

PBS: phosphate-buffered saline

PCR: polymerase chain reaction

PEG: polyethylene glycol

PMSF: phenylmethylsulfonyl fluoride

PNK: polynucleotide kinase

RBV: ribavirin

RdRp: RNA-dependent RNA-polymerase

RMSD: root-mean-square deviation

RNA: ribonucleic acid

RNP: ribonucleoprotein

RT: room temperature

RT-PCR: reverse transcription-polymerase chain reaction

SD: standard deviation

SDS: sodium dodecyl sulfate

SDS-PAGE: polyacrylamide gel electrophoresis

sNSV: segmented negative-ssRNA viruses

SNV: *Sin Nombre virus*

SOC: super optimal broth with catabolite repression

ss: single-stranded

TCEP: tris 2-carboxyethyl phosphine

TEMED: tetramethylethylenediamine

T_m: melting temperature

TULV: *Tula virus*

UTP: uridine triphosphate

UTR: untranslated region

UV: ultraviolet

vRNA: viral ribonucleic acid

wt: wild-type

IX. BIBLIOGRAPHY

Adams, P.D. et al., 2010. PHENIX: A comprehensive Python-based system for macromolecular structure solution. *Acta Crystallographica Section D: Biological Crystallography*, 66(2), pp.213–221.

Angulo, J. et al., 2015. Association of Single-Nucleotide Polymorphisms in *IL28B,* but Not *TNF-a,* With Severity of Disease Caused by Andes Virus. *Clinical Infectious Diseases*, 61, pp.62-69.

Baker, C.M. & Grant, G.H., 2007. Role of aromatic amino acids in protein-nucleic acid recognition. *Biopolymers*, 85, p.456-470.

Baker, N.A. et al., 2001. Electrostatics of nanosystems: Application to microtubules and the ribosome. *Proceedings of the National Academy of Sciences of the United States of America*, 98(18), pp.10037–10041.

Barr, J.N., 2007. Bunyavirus mRNA synthesis is coupled to translation to prevent premature transcription termination. *RNA*, 13(5), pp.731–736.

Battisti, A.J. et al., 2011. Structural studies of Hantaan virus. *Journal of virology*, 85(2), pp.835–41.

Battye, T.G.G. et al., 2011. *iMOSFLM*: a new graphical interface for diffraction-image processing with *MOSFLM*. *Acta Crystallographica Section D Biological Crystallography*, 67(4), pp.271–281.

Baughman, B.. et al., 2012. Identificatin of influenza endonuclease inhibitors using a novel fluorescence polarization assay. *ACS Chemical Biology*, 7(3), pp.526–534.

Bouloy, M., Plotch, S.J. & Krug, R.M., 1978. Globin mRNAs are primers for the transcription of influenza viral RNA in vitro. *Proceedings of the National Academy of Sciences of the United States of America*, 75(10), pp.4886–4890.

Brown, K.S., Ebihara, H. & Feldmann, H., 2012. Development of a minigenome system for Andes virus, a New World hantavirus. *Archives of virology*, 157(11), pp.2227–2233.

Campen, M.J. et al., 2006. Characterization of shock in a hamster model of hantavirus infection. *Virology*, 356(1-2), pp.45–49.

Castro, C. et al., 2009. Nucleic acid polymerases employ a general acid for nucleotidyl transfer. *Nature structural & molecular biology*, 16(2), pp.212–218.

Cheng, E. & Mir, M. a, 2012. Signatures of host mRNA 5' terminus for efficient hantavirus cap snatching. *Journal of virology*, 86(18), pp.10173–10185.

Chiang, C.F. et al., 2014. Small interfering RNA inhibition of andes virus replication. *PLoS ONE*, 9(6), p.e99764.

Custer, D.M. et al., 2003. Active and Passive Vaccination against Hantavirus Pulmonary Syndrome with Andes Virus M Genome Segment-Based DNA Vaccine. *Journal of virology*, 77(18), pp.9894–9905.

Das, K. & Arnold, E., 2015. Negative-Strand RNA Virus L Proteins: One Machine, Many Activities. *Cell*, 162(2), pp.239–241.

DeLano, W., 2002. PyMol: An Open-Source Molecular Graphics Tool. *Ccp4 Protein Crystallography*, (4), 44-53.

Dias, A. et al., 2009. The cap-snatching endonuclease of influenza virus polymerase resides in the PA subunit. *Nature*, 458(7240), pp.914–918.

van Dijk, A.A., Makeyev, E. V. & Bamford, D.H., 2004. Initiation of viral RNA-dependent RNA polymerization. *Journal of General Virology*, 85(5), pp.1077–1093.

Dolinsky, T.J. et al., 2007. PDB2PQR: expanding and upgrading automated preparation of biomolecular structures for molecular simulations. *Nucleic Acids Research*, 35, pp.W522–W525.

Drozdetskiy, A. et al., 2015. JPred4: a protein secondary structure prediction server. *Nucleic Acids Res*, 43(1), pp.389–394.

DuBois, R.M. et al., 2012. Structural and Biochemical Basis for Development of Influenza Virus Inhibitors Targeting the PA Endonuclease. *PLoS Pathogens*, 8(8), p.e1002830.

Easterbrook, J.D. & Klein, S.L., 2008. Immunological mechanisms mediating hantavirus persistence in rodent reservoirs. *PLoS pathogens*, 4(11), p.e1000172.

Emsley, P. et al., 2010. Features and development of Coot. *Acta crystallographica. Section D, Biological crystallography*, 66(Pt 4), pp.486–501.

Ericsson, U.B. et al., 2006. Thermofluor-based high-throughput stability optimization of proteins for structural studies. *Analytical Biochemistry*, 357(2), pp.289–298.

Fontana, J. et al., 2008. The unique architecture of Bunyamwera virus factories around the Golgi complex. *Cellular Microbiology*, 10(10), pp.2012–2028.

Galeno, H. et al., 2002. First human isolate of hantavirus (Andes virus) in the Americas. *Emerging Infectious Diseases*, 8(7), pp.657–661.

Garcin, D. et al., 1995. The 5' ends of Hantaan virus (Bunyaviridae) RNAs suggest a prime-and-realign mechanism for the initiation of RNA synthesis. *Journal of virology*, 69(9), pp.5754–5762.

Gavrilovskaya, I.N. et al., 2002. Pathogenic hantaviruses selectively inhibit b3 integrin directed endothelial cell migration. *Archives of Virology*, 147(10), pp.1913–1931.

Gerlach, P. et al., 2015. Structural Insights into Bunyavirus Replication and Its Regulation by the vRNA Promoter. *Cell*, 161(6), pp.1267–1279.

Haese, N. et al., 2015. Antiviral Biologic Produced in DNA Vaccine/Goose Platform Protects Hamsters Against Hantavirus Pulmonary Syndrome When Administered Post-exposure. *PLOS Neglected Tropical Diseases*, 9(6), p.e0003803.

Heinemann, P., Schmidt-Chanasit, J. & Gunther, S., 2013. The N Terminus of Andes Virus L Protein Suppresses mRNA and Protein Expression in Mammalian Cells. *Journal of Virology*, 87(12), pp.6975–6985.

Hepojoki, J. et al., 2010. Interactions and oligomerization of hantavirus glycoproteins. *Journal of virology*, 84(1), pp.227–242.

Hooper, J.W. et al., 2001. A Lethal Disease Model for Hantavirus Pulmonary Syndrome. *Virology*, 289(1), pp.6–14.

Hooper, J.W. et al., 2014. DNA vaccine-derived human IgG produced in transchromosomal bovines protect in lethal models of hantavirus pulmonary syndrome. *Science translational medicine*, 6(264), p.1-9.

Hooper, J.W. et al., 2006. Hantaan/Andes virus DNA vaccine elicits a broadly cross-reactive neutralizing antibody response in nonhuman primates. *Virology*, 347(1), pp.208–216.

Huiskonen, J.T. et al., 2010. Electron cryotomography of Tula hantavirus suggests a unique assembly paradigm for enveloped viruses. *Journal of virology*, 84(10), pp.4889–4897.

Hutchinson, K.L., Peters, C.J. & Nichol, S.T., 1996. Sin Nombre virus mRNA synthesis. *Virology*, 224(1), pp.139–149.

Ingles-prieto, A. et al., 2013. Conservation of Protein Structure over Four Billion Years. *Structure*, 21(9), p.1690-1697.

Jääskeläinen, K.M. et al., 2007. Tula and Puumala Hantavirus NSs ORFs Are Functional and the Products Inhibit Activation of the Interferon-Beta Promoter. *Journal of Medical Virology*, 79, pp.1527–1536.

Jin, M. et al., 2002. Hantaan virus enters cells by clathrin-dependent receptor-mediated endocytosis. *Virology*, 294(1), pp.60–69.

Jones, S. et al., 2001. Protein-RNA interactions: a structural analysis. *Nucleic Acids Research*, 29(4), pp.943–954.

Jonsson, C.B., Figueiredo, L.T.M. & Vapalahti, O., 2010. A Global Perspective on Hantavirus Ecology, Epidemiology, and Disease. *Clinical Microbiology Reviews*, 23(2), pp.412–441.

Kaukinen, P., Vaheri, A. & Plyusnin, A., 2005. Hantavirus nucleocapsid protein: A multifunctional molecule with both housekeeping and ambassadorial duties. *Archives of Virology*, 150(9), pp.1693–1713.

Kukkonen, S.K.J., Vaheri, A. & Plyusnin, A., 2005. L protein, the RNA-dependent RNA polymerase of hantaviruses. *Archives of Virology*, 150(3), pp.533–556.

Kukkonen, S.K.J., Vaheri, A. & Plyusnin, A., 2004. Tula hantavirus L protein is a 250 kDa perinuclear membrane-associated protein. *Journal of General Virology*, 85(5), pp.1181–1189.

Kwilas, S. et al., 2014. A hantavirus pulmonary syndrome (HPS) DNA vaccine delivered using a spring-powered jet injector elicits a potent neutralizing antibody response in rabbits and nonhuman primates. *Current gene therapy*, 14(3), pp.200–210.

Mackow, E.R. & Gavrilovskaya, I.N., 2001. Cellular receptors and hantavirus pathogenesis. *Current topics in microbiology and immunology*, 256, pp.91–115.

Martinez-valdebenito, C. et al., 2014. Person-to-Person Household and Nosocomial Transmission of Andes. *Emerging infectious diseases*, 20(10), pp.1629–1636.

Mattar, S., Guzmán, C. & Figueiredo, L.T., 2015. Diagnosis of hantavirus infection in humans. *Expert Review of Anti-infective Therapy*, 8, pp.1–8.

McCoy, A.J. et al., 2007. Phaser crystallographic software. *Journal of Applied Crystallography*, 40(4), pp.658–674.

McWilliam, H. et al., 2013. Analysis Tool Web Services from the EMBL-EBI. *Nucleic acids research*, 41, pp.W597–600.

Meissner, J.D. et al., 2002. Complete nucleotide sequence of a Chilean hantavirus. *Virus research*, 89(1), pp.131–143.

Mir, M. a et al., 2006. Hantavirus N protein exhibits genus-specific recognition of the viral RNA panhandle. *Journal of virology*, 80(22), pp.11283–11292.

Monod, A. et al., 2015. Learning from structure-based drug design and new antivirals targeting the ribonucleoprotein complex for the treatment of influenza. *Expert Opinion on Drug Discovery*, 441, pp.345–371.

Moreli, M.L. et al., 2014. Effectiveness of the ribavirin in treatment of hantavirus infections in the Americas and Eurasia: a meta-analysis. *Virusdisease*, 25(3), pp.385–389.

Morin, B. et al., 2010. The N-terminal domain of the arenavirus L protein is an RNA endonuclease essential in mRNA transcription. *PLoS Pathogens*, 6(9), p.e1001038.

Nsoesie, E.O. et al., 2014. Modeling to Predict Cases of Hantavirus Pulmonary Syndrome in Chile. *PLoS Neglected Tropical Diseases*, 8(4), p.e2779.

Ogino, M. et al., 2004. Cell Fusion Activities of Hantaan Virus Envelope Glycoproteins. *Journal of Virology*, 78(19), pp.10776–10782.

Padula, P. et al., 2004. Transmission study of Andes hantavirus infection in wild sigmodontine rodents. *Journal of virology*, 78(21), pp.11972–11979.

Ramanathan, H.N. & Jonsson, C.B., 2008. New and Old World hantaviruses differentially utilize host cytoskeletal components during their life cycles. *Virology*, 374(1), pp.138–150.

Ramsden, C. et al., 2008. High rates of molecular evolution in hantaviruses. *Molecular Biology and Evolution*, 25(7), pp.1488–1492.

Ramsden, C., Holmes, E.C. & Charleston, M. a., 2009. Hantavirus evolution in relation to its rodent and insectivore hosts: No evidence for codivergence. *Molecular Biology and Evolution*, 26(1), pp.143–153.

Ravkov, E. V, Nichol, S.T. & Compans, R.W., 1997. Polarized Entry and Release in Epithelial Cells of Black Creek Canal Virus, a New World Hantavirus. *Journal of virology*, 71(2), pp.1147–1154.

Reguera, J., Cusack, S. & Kolakofsky, D., 2014. Segmented negative strand RNA virus nucleoprotein structure. *Current opinion in virology*, 5, pp.7–15.

Reguera, J., Gerlach, P. & Cusack, S., 2016. Towards a structural understanding of RNA synthesis by negative strand RNA viral polymerases. *Current Opinion in Structural Biology*, 36, pp.75–84.

Reguera, J., Weber, F. & Cusack, S., 2010. Bunyaviridae RNA polymerases (L-protein) have an N-terminal, influenza-like endonuclease domain, essential for viral cap-dependent transcription. *PLoS pathogens*, 6(9), p.e1001101.

Reich, S. et al., 2014. Structural insight into cap-snatching and RNA synthesis by influenza polymerase. *Nature*, 516(7531), pp.361–366.

Rivera, P.C., Gonzalez-Ittig, R.E. & Gardenal, C.N., 2015. Preferential host switching and its relation with Hantavirus diversification in South America. *Journal of General Virology*, pp.2531–2542.

Robert, X. & Gouet, P., 2014. Deciphering key features in protein structures with the new ENDscript server. *Nucleic Acids Research*, 42(W1), pp.W320–W324.

Rowe, R.K., Suszko, J.W. & Pekosz, A., 2008. Roles for the Recycling Endosome, Rab8, and Rab11 in hantavirus release from epithelial cells. *Virology*, 382(2), pp.239–249.

Safronetz, D., Haddock, E., et al., 2011. In vitro and in vivo activity of Ribavirin against Andes virus infection. *PLoS ONE*, 6(8), p.e23560.

Safronetz, D., Zivcec, M., et al., 2011. Pathogenesis and host response in Syrian hamsters following intranasal infection with Andes virus. *PLoS pathogens*, 7(12), p.e1002426.

Saïda, F. et al., 2006. Expression of highly toxic genes in E. coli: special strategies and genetic tools. *Current protein & peptide science*, 7(1), pp.47–56.

Schneider, C. a, Rasband, W.S. & Eliceiri, K.W., 2012. NIH Image to ImageJ: 25 years of image analysis. *Nature Methods*, 9(7), pp.671–675.

Shi, X. & Elliott, R.M., 2004. Analysis of N-Linked Glycosylation of Hantaan Virus Glycoproteins and the Role of Oligosaccharide Side Chains in Protein Folding and Intracellular Trafficking. *Journal of Virology*, 78(10), pp.5414–5422.

Spengler, J.R. et al., 2013. Experimental Andes virus infection in deer mice: characteristics of infection and clearance in a heterologous rodent host. *PloS one*, 8(1), p.e55310.

Steczkiewicz, K. et al., 2012. Sequence, structure and functional diversity of PD-(D/E)XK phosphodiesterase superfamily. *Nucleic acids research*, 40(15), pp.7016–7045.

Vaheri, A. et al., 2013. Uncovering the mysteries of hantavirus infections. *Nature Reviews Microbiology*, 11(8), pp.539–550.

Vera-Otarola, J. et al., 2010. The 3' untranslated region of the Andes hantavirus small mRNA functionally replaces the poly(A) tail and stimulates cap-dependent translation initiation from the viral mRNA. *Journal of virology*, 84(19), pp.10420–10434.

Vera-Otarola, J. et al., 2012. The Andes hantavirus NSs protein is expressed from the viral small mRNA by a leaky scanning mechanism. *Journal of virology*, 86(4), pp.2176–2187.

Vial, P. a et al., 2014. A non-randomized multicentre trial of human immune plasma for treatment of hantavirus cardiopulmonary syndrome by ANDV. *Antiviral Therapy*, 386, pp.377–386.

Vial, P. a. et al., 2013. High-dose intravenous methylprednisolone for hantavirus cardiopulmonary syndrome in Chile: A double-blind, randomized controlled clinical trial. *Clinical Infectious Diseases*, 57(7), pp.943–951.

Vial, P.A. et al., 2006. Incubation period of hantavirus cardiopulmonary syndrome. *Emerging infectious diseases*, 12(8), pp.1271–1283.

Wahl-Jensen, V. et al., 2007. Temporal analysis of Andes virus and Sin Nombre virus infections of Syrian hamsters. *Journal of virology*, 81(14), pp.7449–7462.

Wallat, G.D. et al., 2014. High-resolution structure of the N-terminal endonuclease domain of the Lassa virus L polymerase in complex with magnesium ions. *PLoS ONE*, 9(2), pp.1–10.

Yang, W., 2011. Nucleases: diversity of structure, function and mechanism. *Quarterly reviews of biophysics*, 44, pp.1-93.